Crosstalk between chloroplast protein import and the SUMO system revealed through genetic and molecular investigation

Samuel James Watson[1†], Na Li[1], Yiting Ye[2], Feijie Wu[2,3], Qihua Ling[1,2,3‡], R. Paul Jarvis[1,3]*

[1]Department of Plant Sciences, University of Oxford, Oxford OX1 3RB, UK.

[2]National Key Laboratory of Plant Molecular Genetics, CAS Centre for Excellence in Molecular Plant Sciences, Institute of Plant Physiology and Ecology, Shanghai Institutes for Biological Sciences, Chinese Academy of Sciences, Shanghai, China.

[3]Department of Biology, University of Leicester, Leicester LE1 7RH, UK.

[†]Present address: Cambridge Institute for Therapeutic Immunology and Infectious Disease, Jeffrey Cheah Biomedical Centre, University of Cambridge, Cambridge CB2 0AW, UK.

*For correspondence: paul.jarvis@plants.ox.ac.uk

Abstract

The chloroplast proteome contains thousands of different proteins that are encoded by the nuclear genome. These proteins are imported into the chloroplast via the action of the TOC translocase and associated downstream systems. Our recent work has revealed that the stability of the TOC complex is dynamically regulated by the ubiquitin-dependent chloroplast-associated protein degradation (CHLORAD) pathway. Here, we demonstrate that the stability of the TOC complex is also regulated by the SUMO system. *Arabidopsis* mutants representing almost the entire SUMO conjugation pathway can partially suppress the phenotype of *ppi1*, a pale yellow mutant lacking the Toc33 protein. This suppression is linked to the increased stability of TOC proteins and improvements in chloroplast development. In addition, we demonstrate using molecular and biochemical experiments that the SUMO system directly targets TOC proteins. Thus, we have identified a regulatory link between the SUMO system and chloroplast protein import.

Introduction

The chloroplast is a membrane-bound organelle that houses photosynthesis in all green plants (Jarvis and Lopez-Juez, 2013). Chloroplasts have an unusual evolutionary history – they are the integrated descendants of a cyanobacterial ancestor that entered the eukaryotic lineage via endosymbiosis. Although chloroplasts retain small genomes, almost all of the proteins required for chloroplast development and function are now encoded by the central, nuclear genome (Jarvis, 2008). These proteins must be imported into the organelle after synthesis in the cytosol, and this import is mediated by the coordinate action of the TOC and TIC complexes (the translocons at the outer and inner envelope membranes of chloroplasts) (Jarvis, 2008).

The TOC complex contains three major components: the Omp85 (outer membrane protein, 85 kDa)-related protein, Toc75, which serves as a membrane channel (Schnell et al., 1994; Tranel et al., 1995), and two GTPase-domain receptor proteins, Toc33 and Toc159 (Hirsch et al., 1994; Kessler et al., 1994; Perry and Keegstra, 1994; Jarvis et al., 1998; Jarvis, 2008). Toc33 and Toc159 project into the cytosol and bind incoming preproteins.

The key components of the TOC complex were identified more than two decades ago (Hirsch et al., 1994; Kessler et al., 1994; Schnell et al., 1994; Tranel et al., 1995; Jarvis, 2008). However, the regulation of the activity and stability of the complex was, until recently, poorly understood. Major insights came from a forward genetic screen for suppressors of the pale yellow Toc33 mutant, *ppi1* (Ling et al., 2012). In this screen, SP1 (SUPPRESSOR OF PPI1 LOCUS 1), a novel RING-type E3 ubiquitin ligase, was identified. A series of *sp1* mutations were shown to partially suppress the phenotypic defects of *ppi1* with respect to chlorosis, chloroplast development, and chloroplast protein import. In addition, SP1 function was shown to promote plastid interconversion events (for example, the development of the chloroplast from its precursor organelle, the etioplast). Later work demonstrated that SP1 function is also important for abiotic stress tolerance, by enabling optimisation of the organellar proteome via protein import regulation (Ling and Jarvis, 2015). Thus, through SP1, the ubiquitin-proteasome system promotes TOC complex degradation and reconfiguration in response to developmental and/or environmental stimuli.

Ubiquitinated TOC proteins are extracted from the chloroplast outer envelope membrane and degraded in the cytosol. Recent work identified two proteins that physically associate with SP1 and promote the membrane extraction of TOC proteins (Ling et al., 2019). These are SP2, an Omp85-type β-barrel channel protein that was identified in the same genetic screen as SP1, and Cdc48, a well-characterised cytosolic AAA+ chaperone ATPase that provides the motive force for the extraction of proteins from the chloroplast outer envelope. The three proteins – SP1, SP2 and Cdc48 – together define a new pathway for the ubiquitination, membrane extraction, and degradation of chloroplast outer envelope proteins, which has been named chloroplast-associated protein degradation, or CHLORAD. In addition to CHLORAD, there exist cytosolic ubiquitin-dependent systems that also contribute to chloroplast biogenesis, by regulating the levels of unimported preproteins (Lee et al., 2009; Grimmer et al., 2020), and by controlling the stability of the Toc159 receptor prior to its integration into the outer envelope membrane (Shanmugabalaji et al., 2018).

The discovery of SP1 and the CHLORAD pathway demonstrated that the TOC complex is not static but, instead, can be rapidly ubiquitinated and degraded in response to developmental and environmental stimuli. To complement this work, we decided to explore whether the TOC complex is also regulated by the SUMO system. This work was motivated by the results of a high-throughput screen for SUMO substrates in *Arabidopsis* (Elrouby and Coupland, 2010). This screen suggested that Toc159, a key component of the TOC complex, is a SUMO substrate. SUMOylation is intricately

involved in plant development and stress adaptation, and so we were interested to determine whether the TOC complex is targeted by the SUMO system, and whether any such SUMOylation is functionally important. As crosstalk between the SUMO system and the ubiquitin-proteasome system is common, we reasoned that answering these questions might provide insights into the regulation of SP1 and the CHLORAD pathway.

To explore the relationship between chloroplast protein import and the SUMO system, we carried out a comprehensive series of genetic, molecular and biochemical experiments. Mutants representing most components of the *Arabidopsis* SUMO pathway were found to partially suppress the phenotype of the chlorotic Toc33 null mutant, *ppi1*, with respect to leaf chlorophyll accumulation, chloroplast development, and TOC protein abundance. Conversely, overexpression of either *SUMO1* or *SUMO3* enhanced the severity of the *ppi1* phenotype. Moreover, the E2 SUMO conjugating enzyme, SCE1, was found to physically interact with the TOC complex in bimolecular fluorescence complementation experiments; and TOC proteins were seen to physically associate with SUMO proteins in immunoprecipitation assays. In combination, our data conclusively demonstrate significant crosstalk between the SUMO system and chloroplast protein import, and emphasise the complexity of the regulation of the TOC translocase.

Results

The E2 SUMO conjugating enzyme mutant *sce1-4*, and the E3 SUMO ligase mutants *siz1-4* and *siz1-5*, partially suppress the phenotype of Toc33 mutant, *ppi1*

Two key components of the CHLORAD pathway, SP1 and SP2, were identified in a forward genetic screen for suppressors of *ppi1,* an *Arabidopsis* Toc33 null mutant (Ling et al., 2012; Ling et al., 2019). Both *sp1* and *sp2* mutants can partially suppress the *ppi1* phenotype with respect to chlorophyll accumulation, chloroplast development, and TOC protein abundance. To investigate whether the TOC complex is targeted by the SUMO system, we obtained several *Arabidopsis* SUMO system mutants, crossed them with *ppi1*, and carefully examined the phenotypes of the resulting double mutants. This reverse genetic approach was possible because the basic architecture of the *Arabidopsis* SUMO system is remarkably simple. In the SUMO pathway, the ubiquitin-like SUMO modifier protein is conjugated to substates by the coordinated action of E1 activating enzymes, E2 conjugating enzymes, and E3 SUMO ligases. Although thousands of proteins are SUMOylated in *Arabidopsis*, there is just one known E1 SUMO activating enzyme, one known E2 SUMO conjugating enzyme, and only two known E3 SUMO ligases of canonical function (Saracco et al., 2007; Ishida et al., 2009).

First, we analysed *sce1-4*, a weak mutant allele of the sole E2 SUMO conjugating enzyme gene in *Arabidopsis*, which is an essential gene (Saracco et al., 2007). The *sce1-4* mutant shows a moderate reduction in the expression of SCE1 and in global levels of SUMOylation, but it displays no obvious visible phenotypic defects under steady-state conditions (Saracco et al., 2007). The *ppi1 sce1-4* double mutant was phenotypically characterised, and, intriguingly, it appeared greener than the *ppi1* single mutant (Figure 1A; Figure 1 – Supplement 1A). This was linked to a moderate increase in leaf chlorophyll concentration (Figure 1B; Figure 1 – Supplement 1B). Next, we asked whether the phenotypic suppression observed in *ppi1 sce1-4* was linked to changes in the development of chloroplasts. The chloroplasts of *ppi1 sce1-4* were visualised via transmission electron microscopy. Interestingly, the chloroplasts of the *ppi1 sce1-4* double mutant appeared larger and better developed than those of the *ppi1* control (Figure 1C). The transmission electron micrographs were quantitatively analysed, and the *ppi1 sce1-4* chloroplasts were indeed found to be significantly larger

116 than those of *ppi1* (Figure 1D), with larger, more interconnected thylakoidal granal stacks (Figures 1E
117 and 1F).

118 SUMO conjugation is usually dependent on the action of E3 SUMO ligases. In *Arabidopsis*, the best
119 characterised E3 SUMO ligase is SIZ1 (Kurepa et al., 2003; Miura et al., 2005; Saracco et al., 2007).
120 SIZ1 is not essential, but null mutants display severely dwarfed phenotypes. In order to include SIZ1
121 in our genetic analysis, we obtained two new T-DNA insertion alleles, and named them *siz1-4* and
122 *siz1-5.* While both mutants were visibly similar to the published mutants (Miura et al., 2005; Liu et
123 al., 2019), *siz1-4* showed a milder phenotype with only moderate growth retardation when grown to
124 maturity. We mapped the integration sites of the T-DNA insertions in these two mutants (Figure 1 –
125 Supplement 2A), and showed that both display a strong reduction in *SIZ1* transcript by RT-PCR
126 analysis (Figure 1 – Supplement 2B). In addition, both mutants displayed defects in global
127 SUMOylation in response to heat shock, similar to the published alleles (Figure 1 – Supplement 3).
128 The two new *siz1* mutants were crossed with *ppi1* and the resulting double mutants were
129 phenotypically characterised. Both the *ppi1 siz1-4* and the *ppi1 siz1-5* double mutants appeared
130 greener than the *ppi1* control (Figure 1G; Figure 1 – Supplement 1C). In addition, the double mutants
131 showed dramatic increases in leaf chlorophyll concentration relative to *ppi1* (Figure 1H; Figure 1 –
132 Supplement 1D). Next, we asked whether the phenotypic suppression observed in *ppi1 siz1-4* and
133 *ppi1 siz1-5* was linked to changes in the abundance of TOC proteins. To this end, protein samples
134 were taken from the two double mutants and relevant control plants and resolved via
135 immunoblotting. Both double mutants displayed clear increases in the abundance of Toc159 and
136 Toc75, two core components of the TOC complex, relative to *ppi1* (Figures 1I, 1J, and 1K).

137 **The suppression effects mediated by the SUMO system mutants are specific**

138 As discussed in the previous section, the SUMO system is encoded by a remarkably small number of
139 genes in *Arabidopsis*. As a consequence, SUMO system mutants have highly pleiotropic molecular
140 and physiological phenotypes. We therefore asked whether the partial suppression of *ppi1* by SUMO
141 system mutants was specific to the *ppi1* background. We crossed *sce1-4* with *tic40-4* and *hsp93-V-1*,
142 two TIC-complex-associated mutants. These mutants are chlorotic, due to defects in protein import
143 across the chloroplast inner membrane, and in this respect are highly similar to *ppi1* (Kovacheva et
144 al., 2005). Significantly, the resulting double mutants, *tic40-4 sce1-4* and *hsp93-V-I sce1-4*, were
145 indistinguishable from *tic40-4* and *hsp93-V-1*, their respective single mutant controls (Figures 2A and
146 2C). Moreover, the double mutants did not display changes in leaf chlorophyll accumulation relative
147 to the single mutant controls (Figures 2B and 2D). We therefore concluded that the suppression
148 effects observed in *ppi1 sce1* plants were background-specific and associated with the TOC complex.

149 Next, we asked whether the *sce1-4* and *siz1-4* single mutants display an increase in chlorophyll
150 concentration even in the wild-type background. However, neither mutant appeared greener than
151 wild-type plants (Figures 2E and 2G; Figure 1 – Supplement 1A and 1C) or displayed an increase in
152 leaf chlorophyll concentration (Figures 2F and 2H; Figure 1 – Supplement 1B and 1D). We therefore
153 concluded that the suppression effects mediated by the SUMO mutants were synthetic phenotypes
154 specific to the *ppi1* background.

155 **BiFC analysis reveals that SCE1 physically interacts with TOC proteins**

156 Our reverse genetic experiments revealed a genetic interaction between the E2 SUMO conjugating
157 enzyme, SCE1, and protein import across the chloroplast outer membrane. To determine whether
158 SCE1 directly interacts with the TOC complex, we carried out bimolecular fluorescence
159 complementation (BiFC) experiments in *Arabidopsis* protoplasts. The *SCE1* coding sequence was

160 cloned into a vector that C-terminally appends the C-terminal half of YFP (cYFP) to its insert. This
161 construct was co-expressed with various other constructs encoding TOC proteins bearing the
162 complementary, N-terminal moiety of the YFP protein (nYFP), appended N-terminally; or with a
163 negative control construct encoding ΔOEP7 bearing the nYFP moiety appended C-terminally. In this
164 system, protein-protein interactions are inferred via the detection of a YFP signal, caused by the
165 nYFP and cYFP fragments coming together to reconstitute a functional YFP protein.

166 Strikingly, SCE1-nYFP was found to physically associate with all tested TOC proteins – nYFP-Toc159,
167 nYFP-Toc132, nYFP-Toc34 and nYFP-Toc33 (Figure 3). Moreover, these interactions were
168 concentrated at the periphery of the chloroplasts, placing them in an appropriate subcellular context
169 for the *in situ* regulation of the chloroplast protein import machinery. Conversely, SCE1-cYFP was not
170 found to physically associate with the negative control protein ΔOEP7-nYFP. The ΔOEP7 protein
171 comprises the transmembrane domain of plastid protein OEP7, which is sufficient to efficiently
172 target the full-length YFP protein to the chloroplast outer membrane (Lee et al., 2001); thus cYFP-
173 ΔOEP7 serves as a location-specific negative control.

174 **Manipulating the expression of three SUMO isoforms alters the phenotypic severity of *ppi1***

175 To further explore the genetic interaction between chloroplast protein import and the SUMO
176 system, we crossed *ppi1* with several SUMO protein mutants. There are three major SUMO isoforms
177 in *Arabidopsis* – SUMO1, SUMO2, and SUMO3. The *SUMO1* and *SUMO2* genes are expressed at a
178 relatively high level throughout the plant and are largely functionally redundant (Saracco et al.,
179 2007; van den Burg et al., 2010). In addition, they are highly similar to each other in terms of amino
180 acid sequence (Saracco et al., 2007). In contrast, at steady state, *SUMO3* is expressed at a relatively
181 low level throughout the plant, while the SUMO3 amino acid sequence is significantly divergent with
182 respect to the other two SUMO isoforms (van den Burg et al., 2010).

183 First, we analysed *SUMO1* and *SUMO2*. We obtained *sum1-1* and *sum2-1*, two previously
184 characterised null mutants (Saracco et al., 2007), and crossed them with *ppi1*. To account for the
185 functional redundancy between these two genes, we also sought a *ppi1 sum1-1 sum2-1* triple
186 mutant. However, as *SUMO1* and *SUMO2* are collectively essential, *ppi1 sum1-1 sum2-1* plants that
187 were homozygous with respect to *ppi1* and *sum2-1*, but heterozygous with respect to the *sum1-1*
188 mutation, were selected from a segregating population. The double and triple mutants were
189 phenotypically characterised, and all three appeared larger and greener than the *ppi1* control plants
190 (Figure 4A). Moreover, the double and triple mutants showed corresponding increases in leaf
191 chlorophyll concentration, with the triple mutant showing a larger increase than the double mutants
192 (Figure 4B). These were synthetic effects, as the *sum1-1*, *sum2-1*, and *sum1-1 sum2-1* single and
193 double mutants did not appear greener than wild-type plants, or show increases in chlorophyll
194 accumulation (Figure 4 – Supplement 1). We therefore concluded that the *sum1-1* and *sum2-1*
195 mutants can additively suppress the phenotype of *ppi1*.

196 To complement the preceding experiment, we generated transgenic plants overexpressing *SUMO1*
197 in the *ppi1* background. The *SUMO1* coding sequence was cloned into a vector carrying a strong,
198 constitutive promotor (cauliflower mosaic virus 35S) upstream of the cloning site. The resulting
199 construct was stably introduced into the *ppi1* background via *Agrobacterium*-mediated
200 transformation. Two lines carrying a single, homozygous transgene insert were identified and taken
201 forward for analysis. The overexpression of *SUMO1* was confirmed in both lines by RT-PCR (Figure 4
202 – Supplement 2A). Significantly, both lines displayed an accentuation of the *ppi1* phenotype: the
203 plants were significantly smaller and paler than the *ppi1* control plants (Figure 4C), and showed
204 decreases in leaf chlorophyll concentration (Figure 4D).

205 Next, we turned our attention to *SUMO3*. We obtained *sum3-1*, a previously characterised null
206 mutant (van den Burg et al., 2010), and crossed it with *ppi1*. The resulting double mutant was
207 phenotypically characterised, but it did not appear obviously different from the *ppi1* control (Figure
208 4E). Correspondingly, it did not display any clear increase in leaf chlorophyll concentration relative to
209 *ppi1* (Figure 4F). To complement this experiment, we generated transgenic plants overexpressing
210 *SUMO3* in the *ppi1* background, using the approach described above, and a line carrying a single,
211 homozygous insert was identified and taken forward for analysis. The overexpression of *SUMO3* was
212 confirmed by RT-PCR (Figure 4 – Supplement 2B). Interestingly, the transgenic plants showed a
213 striking increase in the severity of the *ppi1* phenotype: the plants were severely dwarfed and paler
214 than the *ppi1* control (Figure 4G), and displayed a significant decrease in leaf chlorophyll
215 accumulation (Figure 4H). These findings are particularly noteworthy when considered alongside a
216 previous report which explored the consequences of overexpressing *SUMO3* in wild-type plants (van
217 den Burg et al., 2010). In that study, *SUMO3* overexpression was not found to alter the appearance
218 of the transgenic plants, which implies a degree of specificity in the phenotypic accentuation
219 observed here.

220 **Biochemical analysis reveals SUMOylation of TOC proteins *in vivo***

221 The genetic and molecular experiments described thus far strongly suggested that TOC proteins are
222 SUMOylated. However, to our knowledge, conclusive evidence that chloroplast-resident proteins are
223 SUMOylated is currently lacking. To investigate whether chloroplast proteins may be SUMOylated,
224 we isolated chloroplasts from seedlings by cell fractionation and analysed them by anti-SUMO
225 immunoblotting. For this analysis, we employed a proven commercial antibody against SUMO1,
226 which is one of the most abundant SUMO isoforms in *Arabidopsis* making it more tractable for
227 analysis, and which furthermore is known to accumulate in response to heat and other stresses
228 (Kurepa et al., 2003; van den Burg et al., 2010). To enhance detection of SUMOylated proteins in our
229 samples, we subjected some of the seedlings to heat shock before chloroplast isolation and/or
230 treatment with 10 mM N-ethylmaleimide (NEM) during chloroplast isolation. NEM is a potent
231 inhibitor of SUMO-specific proteases (Hilgarth and Sarge, 2005). Importantly, we detected protein
232 SUMOylation in the isolated chloroplast samples, and this SUMOylation was increased by NEM
233 treatment (Figure 5 – Supplement 1).

234 Next, we carried out a series of biochemical experiments to determine whether TOC proteins are
235 SUMOylated. In the first of these, the *SCE1* coding sequence was cloned into a vector that appends a
236 C-terminal YFP tag (Karimi et al., 2002). We confirmed that the resulting SCE1-YFP construct delivers
237 good expression and the expected nucleocytoplasmic fluorescence pattern when transiently
238 expressed in protoplasts (Figure 5 – Supplement 2A). Then, we transfected a large volume of
239 protoplasts with the SCE1-YFP construct (or with a YFP-HA negative control construct), and
240 performed immunoprecipitation (IP) using YFP-Trap magnetic beads. The samples were analysed by
241 immunoblotting. The YFP-HA and SCE1-YFP fusion proteins both showed robust expression and
242 strong recovery in the IP elutions (Figure 5A). Remarkbly, the SCE1-YFP fusion protein was found to
243 be associated with native Toc159 and Toc132, but not with the negative control proteins Tic110 or
244 Tic40 (Figure 5A). Conversely, YFP-HA did not associate with any of the tested proteins. Given that
245 SCE1 is a promiscuous enzyme that associates with thousands of proteins (Elrouby and Coupland,
246 2010), and that these interactions are likely to be transient, it is remarkable that TOC co-elution was
247 detectable in this experiment.

248 In the second experiment, we cloned the *SUMO1*, *SUMO2* and *SUMO3* coding sequences into a
249 vector that appends an N-terminal YFP tag to its insert (Karimi et al., 2002), a modification which
250 previous studies have shown to be tolerated (Ayaydin and Dasso, 2004). All three constructs

251 expressed well and showed the expected nucleocytoplasmic fluorescence pattern when transiently
252 expressed in protoplasts (Figure 5 – Supplement 2B). The three constructs were expressed in parallel
253 in protoplasts alongside the YFP-HA negative control construct. As in the previous experiment, the
254 protoplasts were subjected to YFP-Trap immunoprecipitation, and the samples were subsequently
255 analysed by immunoblotting. Remarkably, all three YFP-SUMO proteins were found to physically
256 associate with Toc159, although YFP-SUMO3 clearly bound Toc159 with the greatest affinity (Figure
257 5B; Figure 5 – Supplement 3). Moreover, inspection of an extended exposure of the anti-YFP blot
258 revealed a number of higher molecular weight bands that we interpret to be SUMO adducts and
259 indicative of the functionality of the fusions (Figure 5 – Supplement 4). In contrast with the SUMO
260 fusions, the YFP-HA negative control did not associate with Toc159, and none of the four YFP fusion
261 proteins physically associated with Tic40, a negative control protein (Figure 5B).

262 The immunoprecipitation experiment described above identified SUMO3 as having the highest
263 affinity for Toc159. To extend our analysis of SUMO3 to include another TOC proteins, and to
264 provide more direct evidence for TOC protein SUMOylation, the experiment was repeated with
265 modifications, as follows. Protoplasts were co-transfected with YFP-SUMO3 and Toc33-HA, or YFP-
266 HA and Toc33-HA; in each case, Toc33 was transiently overexpressed to aid detection of this
267 component and its adducts. Upon co-expression of these construct pairs, the protoplast samples
268 were subjected to YFP-Trap immunoprecipitation analysis, as described earlier. In accordance with
269 the Toc159 result (Figure 5B), YFP-SUMO3, but not YFP-HA, was found to physically associate with
270 Toc33-HA (Figure 5C). Moreover, bands of the exact expected molecular weight for Toc33-HA
271 bearing one or two YFP-SUMO3 moieties (75 and 114 kDa) were also detected. These bands were
272 accompanied by a high molecular weight smear at the top of the immunoblot, which is indicative of
273 complex, multisite or chain SUMOylation.

274 Discussion

275 This work has revealed a genetic and molecular link between the SUMO system and chloroplast
276 protein import. The genetic experiments demonstrated that SUMO system mutations can suppress
277 the phenotype of the Toc33 mutant, *ppi1*, while the molecular and biochemical experiments
278 indicated that TOC proteins associate with key SUMO system proteins and are SUMOylated. Visible
279 suppression effects observed in the *ppi1* / SUMO system double mutants were linked to
280 improvements in chloroplast development and enhanced accumulation of key TOC proteins. Thus,
281 our results suggest that SUMOylation acts to destabilise the TOC complex, and that when such
282 SUMOylation is perturbed the TOC proteins are stabilised. We interpret that TOC complexes
283 containing Toc34, Toc75 and Toc159 accumulate at higher levels in *ppi1* / SUMO system double
284 mutants, and that this synthetically improves the double mutant phenotypes relative to the *ppi1*
285 control. Importantly, each core TOC protein, including all of those analysed in this study, was
286 predicted with high probability to have one or more SUMOylation sites (Table 1) (Zhao et al., 2014;
287 Beauclair et al., 2015).

288 The *ppi1* suppression effects described here are remarkably similar to those mediated by the *sp1*
289 and *sp2* mutations (Ling et al., 2012; Ling et al., 2019). Like *sp1* and *sp2*, SUMO system mutations can
290 partially suppress *ppi1* with respect to chlorophyll concentration, TOC protein accumulation, and
291 chloroplast development. This similarity suggests that SUMOylation may regulate the activity of the
292 CHLORAD pathway. This is an attractive hypothesis, as both SUMOylation and the CHLORAD
293 pathway are activated by various forms of environmental stress (Kurepa et al., 2003; Ling and Jarvis,
294 2015; Ling et al., 2019). One possibility is that the SUMOylation of TOC proteins promotes their
295 CHLORAD-mediated degradation. Indeed, as already noted, the ability to carry out SUMOylation is

negatively correlated with the stability of TOC proteins in the context of the developed plants studied here. However, it should be kept in mind that SUMOylation can both promote and antagonise the effects of ubiquitination, in different situations (Desterro et al., 1998; Ahner et al., 2013; Liebelt and Vertegaal, 2016); and so our results do not preclude the possibility that SUMOylation may have different consequences for chloroplast biogenesis in other contexts. The Toc159 receptor is regulated by SP1 when integrated into the outer envelope membrane (Ling et al., 2012; Ling et al., 2019), but by a different E3 ligase when it exists as a cytosolic precursor during the earliest stages of development before germination (Shanmugabalaji et al., 2018). Thus, regulation by SUMOylation might be similarly different in these two distinct developmental contexts.

The precise mechanisms underpinning the observed negative regulation of the TOC apparatus by SUMOylation are currently unknown. One possibility is that the SUMOylation of TOC proteins promotes their association with SP1. SUMOylation can modify protein-protein interactions, and some RING-type E3 ubiquitin ligases specifically recognise SUMOylated substrates (Sriramachandran and Dohmen, 2014). However, these SUMO-targeted ubiquitin ligases (STUbLs) typically contain SUMO-interacting motifs (SIMs) which guide the ligases to SUMO proteins conjugated to their substrates, and these are not apparent in SP1 (data not shown) (Zhao et al., 2014). However, SP1 forms a complex with SP2 and very likely additional cofactors, and these could hypothetically provide a SUMO binding interface. Another possibility is that SUMOylation could be involved in the recruitment of Cdc48 from the cytosol. Two important Cdc48 cofactors are Ufd1 and Npl4, and the former contains a SUMO-interacting motif which can guide Cdc48 to SUMOylated proteins (Nie et al., 2012; Baek et al., 2013). Moreover, the SUMO-mediated recruitment of Cdc48 has important roles in the maintenance of genome stability in yeast (Bergink et al., 2013).

The biochemical experiments described in this manuscript indicate that, of the three SUMO isoforms tested, SUMO3 binds TOC proteins with the highest affinity. However, there is an apparent incongruence between the results of these experiments and the results of the genetic experiments. While the *sum1-1* and *sum2-1* mutants were found to additively suppress *ppi1*, the *sum3-1* mutant did not suppress *ppi1*. At face value, this seems puzzling; however, it can be explained by the relative abundance of the three SUMO proteins *in planta*. SUMO1 and SUMO2 are highly abundant relative to SUMO3, which is, at steady state, very weakly abundant (van den Burg et al., 2010). The immunoprecipitation data shown in Figure 5B indicated that SUMO1 and SUMO2 can weakly interact with Toc159, and so it is likely that these two isoforms can compensate for the loss of SUMO3 in the *sum3-1* mutant. Although SUMO3 associates with TOC proteins with the highest affinity, the higher abundance of the other two SUMO proteins may facilitate such compensation. It is also noteworthy that, when overexpressed, SUMO3 accentuates the *ppi1* phenotype to a far greater extent than does SUMO1.

It is now well established that the regulation of chloroplast protein import has critical roles in plant development and stress acclimation (Sowden et al., 2018; Watson et al., 2018). Here, we demonstrate regulatory crosstalk between the SUMO system and chloroplast protein import, and present results which are consistent with a model in which SUMOylation modulates the activity or effects of the CHLORAD pathway. The precise nature of the links between these two critically important control systems will be the subject of future investigation.

Materials and methods

Plant material and growth conditions

339 All *Arabidopsis thaliana* plants used in this work were of the Columbia-0 (Col-0) ecotype. The
340 mutants used in most of the analyses (*ppi1*, *sce1-4*, *sum1-1*, *sum2-1*, *sum3-1*, *hsp93-V-I*, *tic40-4*)
341 have been described previously (Jarvis et al., 1998; Kovacheva et al., 2005; Saracco et al., 2007; van
342 den Burg et al., 2010). The *siz1-4* (SAIL_805_A10) and *siz1-5* (SALK_111280) mutants were obtained
343 from the Salk Institute Genomic Analysis Laboratory (SIGnAL) (Alonso et al., 2003), via the
344 Nottingham *Arabidopsis* Stock Centre (NASC). Each line was verified via PCR genotyping (see Table 2
345 for primer sequences) and phenotypic analysis (including the double and triple mutants). The
346 positions of the T-DNA insertions were mapped via PCR. The following primer pairs were used to
347 generate diagnostic amplicons from gDNA: LB1 and Siz1-Seq-1R (for mapping *siz1-4*), and LBb1 and
348 Siz1-Seq-3R (for mapping *siz1-5*) (see Table 2D and 2E). The amplicons were sequenced and the
349 positions of the T-DNA insertions inferred from the sequence data.

350 In most experiments, plants were grown on soil (80% (v/v) compost (Levington M2), 20% (v/v)
351 vermiculite (Sinclair Pro, medium particle size)). However, where plants were grown for selection of
352 transformants or for chloroplast isolation, seeds were surface sterilised and sown on petri plates
353 containing Murashige-Skoog (MS) agar medium. The plates were stored at 4°C for 48 hours before
354 being transferred to a growth chamber. Both soil-grown and plate-grown plants were kept in a
355 growth chamber (Percival Scientific) under long-day conditions (16 hours light, 8 hours dark). The
356 light intensity was approximately 120 µE m^{-2} s^{-1}, the temperature was held constant at 20°C, and the
357 humidity was held constant at approximately 70% (relative humidity).

358 **Chlorophyll measurements**

359 Chlorophyll measurements were taken from mature rosette leaves in each instance. A handheld
360 Konica-Minolta SPAD-502 meter was used to take each measurement, and the raw values were
361 converted into chlorophyll concentration values (nmol/mg tissue) via published calibration
362 equations (Ling et al., 2011).

363 **Chloroplast isolation and protein extraction**

364 Chloroplasts were isolated from 14-day-old, plate-grown seedlings as described previously (Flores-
365 Pérez and Jarvis, 2017). Some of the seedlings were heat-shocked immediately prior to chloroplast
366 isolation. To do this, the plates containing the seedlings were wrapped in clingfilm and placed into a
367 water bath (42°C for one hour, followed by a one hour recovery period at 22°C). Protein samples
368 were prepared from the isolated chloroplasts by extraction using SDS-PAGE sample buffer, as well as
369 from whole 14-day-old seedlings as previously described (Kovacheva et al., 2005). In some cases, the
370 samples were treated with 10 mM N-ethylmaleimide (Hilgarth and Sarge, 2005); this was added
371 directly to the protein extraction buffer (whole seedling samples), or to the chloroplast isolation
372 buffer following polytron homogenization and all subsequent buffers (chloroplast samples).

373 **Plasmid constructs**

374 The constructs used in the BiFC experiments were generated as follows. The coding sequences of
375 *SCE1*, *SIZ1*, *TOC159*, *TOC132*, *TOC34* and *TOC33* were PCR amplified from wild-type cDNA (see Table
376 2 for primer sequences). In the case of *ΔOEP7*, the first 105 base pairs of the *OEP7* coding sequence
377 were amplified; this encodes a truncated sequence which is sufficient to efficiently target the full-
378 length YFP protein to the chloroplast outer envelope membrane (Lee et al., 2001). The inserts were
379 cloned into one of the following complementary vectors: pSAT4(A)-cEYFP-N1 (*SCE1*), pSAT4-nEYFP-
380 C1 (*TOC159*, *TOC132*, *TOC34*, *TOC33*), or pSAT4(A)-nEYFP-N1 (*ΔOEP7*), which were described
381 previously (Tzfira et al., 2005; Citovsky et al., 2006).

382 The constructs used in the immunoprecipitation experiments were generated as follows. The coding
383 sequences of *SCE1*, *SUMO1*, *SUMO2* and *SUMO3* were PCR amplified from wild-type cDNA using
384 primers bearing 5' attB1 and attB2 adaptor sequences (see Table 2 for primer sequences). The
385 amplicons were then cloned into pDONR221 (Invitrogen), a Gateway entry vector. The inserts from
386 the resulting entry clones were then transferred to one of two destination vectors: p2GWY7 (*SCE1*)
387 or p2YGW7 (*SUMO1*, *SUMO2*, *SUMO3*); the former appends a C-terminal YFP tag to its insert, and
388 the latter appends an N-terminal YFP tag to its insert (Karimi et al., 2002; Karimi et al., 2005). The
389 Toc33-HA and YFP-HA constructs have been described previously (Ling et al., 2019).

390 The constructs used to generate transgenic plants were generated as follows. The coding sequences
391 of *SUMO1* and *SUMO3* were PCR amplified from wild-type cDNA using primers bearing 5' attB1 and
392 attB2 adaptor sequences (see Table 2 for primer sequences). The inserts were then cloned into
393 pDONR201 (Invitrogen), a Gateway entry vector. The inserts from the resulting entry clones were
394 then transferred to the pH2GW7 binary destination vector (Karimi et al., 2002; Karimi et al., 2005).

395 **Transient expression assays**

396 Protoplasts were isolated from mature rosette leaves of wild-type *Arabidopsis* plants and
397 transfected in accordance with an established method (Wu et al., 2009; Ling et al., 2012). In the BiFC
398 experiments, 100 µL protoplast suspension (containing approximately 10^5 protoplasts) was
399 transfected with 5 µg plasmid DNA; in the immunoprecipitation experiments, 600 µL protoplast
400 suspension (containing approximately 6×10^5 protoplasts) was transfected with 30 µg plasmid DNA.
401 In both cases, the samples were analysed after 15-18 hours.

402 **Stable plant transformation**

403 Transgenic lines carrying the *SUMO1-OX* or *SUMO3-OX* constructs were generated via
404 *Agrobacterium*-mediated floral dip transformation (Clough and Bent, 1998). Transformed plants (T_1
405 generation) were selected on MS medium containing phosphinothricin. Multiple T_2 families were
406 analysed in each case, and lines bearing a single T-DNA insertion were taken forward for further
407 analysis. Transgene expression was analysed by semi-quantitative RT-PCR as described previously
408 (Kasmati et al., 2011) (see Table 2 for primer sequences).

409 **Transmission electron microscopy**

410 Transmission electron micrographs were recorded using mature rosette leaves as previously
411 described (Huang et al., 2011). Images were taken from three biological replicates (different leaves
412 from different individual plants), and at least 10 images were taken per replicate. The images were
413 analysed using ImageJ (Schneider et al., 2012). The freehand tool was used to measure the plan area
414 of the chloroplasts. For this, between 9 and 28 chloroplasts were analysed for each biological
415 replicate (i.e., for each plant), and then an average value for each replicate was calculated and used
416 for statistical comparisons. The analysis of chloroplast ultrastructure was performed as in previous
417 work (Huang et al., 2011). For this, between 3 and 8 chloroplasts were analysed per biological
418 replicate, and the data were processed as above.

419 **BiFC experiments**

420 The BiFC experiments were carried out as described previously (Ling et al., 2019). Protoplasts were
421 co-transfected with two constructs encoding fusion proteins bearing complementary fragments of
422 the YFP protein (nYFP and cYFP) (Citovsky et al., 2006). After transfection and overnight incubation,
423 the protoplasts were imaged using a Leica TCS SP5 laser scanning confocal microscope equipped
424 with a Leica HC Plan Apochromat CS2 63.0x UV water immersion lens with a numerical aperture

425 (N.A.) of 1.2. YFP was excited with an Argon-ion laser at 514 nm, selected using an acousto-optic
426 tuneable filter (AOTF), and was detected using a 525-600 nm bandpass filter and a photomultiplier.
427 Chlorophyll fluorescence was simultaneously excited with 514 nm excitation and detected with a
428 680-700 nm bandpass filter using a photomultiplier. Images were collected in 8-bit resolution with
429 the pinhole set at 111.5 µm (1 Airy Unit), using 16-line averaging and a scan speed of 400 Hz. The
430 image size was 512 x 512 pixels, with an (x,y) pixel size of 0.239 µm. Images were processed in the
431 Leica Application Suite (LAS) software.

432 **Immunoblotting and immunoprecipitation**

433 Protein extraction and immunoblotting were performed as described previously (Kovacheva et al.,
434 2005). Total protein samples were extracted from 50 mg of intact, pooled seedlings after two weeks
435 of growth. To detect proteins, we used an anti-SUMO1 antibody (Ab5316, Abcam), an anti-Toc75-III
436 antibody (Kasmati et al., 2011), an anti-Toc159 antibody (Bauer et al., 2000), an anti-Toc132
437 antibody (Ling et al., 2012), an anti-Toc33 antibody (Kasmati et al., 2011), an anti-Tic110 antibody
438 (Aronsson et al., 2010), an anti-Tic40 antibody (Kasmati et al., 2011), and an anti-green fluorescent
439 protein antibody (Sigma, SAB4301138). In most cases, the secondary antibody used was goat anti-
440 rabbit immunoglobulin G (IgG) conjugated with horseradish peroxidase (Sigma, 12-348); and protein
441 bands were visualised via chemiluminescence using an ECL Plus Western blotting detection kit (GE
442 Healthcare) and an LAS-4000 imager (Fujifilm). However, in the case of Figure 5 – Supplement 1, the
443 secondary antibody was goat anti-rabbit IgG conjugated with alkaline phosphatase (Sigma, A3687),
444 and the membrane was incubated with BCIP/NBT chromogenic substrate (Sigma, B3679).

445 The immunoprecipitation (IP) experiments were carried out as described previously (Ling et al.,
446 2019). Constructs encoding YFP-conjugated fusion proteins (YFP-HA, SCE1-YFP, YFP-SUMO1, YFP-
447 SUMO2, YFP-SUMO3) were transiently expressed in protoplasts. In some cases, the constructs were
448 co-expressed with a construct encoding Toc33-HA. The protoplasts were solubilised using IP buffer
449 containing 1% Triton X-100, and the resulting lysates were incubated with GFP-Trap beads
450 (Chromotek). After four washes in IP buffer, the protein samples were eluted by boiling in SDS-PAGE
451 loading buffer, and then analysed by immunoblotting.

452 **Statistical analysis**

453 The data from each experiment were analysed in R. In most cases, two-tailed T-tests were
454 performed. However, in one case, a one-way ANOVA was performed in conjunction with a Tukey
455 HSD test (as indicated in the figure legend). The figures are annotated to indicate the level of
456 significance, as follows: ns, not significant; *, $p<0.05$; **, $p<0.01$; ***, $p<0.001$; ****, $p<0.0001$;
457 *****, $p<0.00001$.

458 **SUMO site prediction**

459 The amino acid sequences of Toc159, Toc132, Toc120, Toc90, Toc75, Toc33 and Toc34 were
460 retrieved from The *Arabidopsis* Information Resource (TAIR) website (Berardini et al., 2015). The
461 GPS-SUMO algorithm was applied to all seven sequences (http://sumosp.biocuckoo.org/online.php)
462 (Zhao et al., 2014). The 'high stringency' setting was applied. The *p*-values were generated by the
463 GPS-SUMO algorithm, and hits that were accompanied by *p*-values exceeding $p>0.05$ were manually
464 removed. The JASSA algorithm was also applied to all seven amino acid sequences
465 (http://www.jassa.fr/index.php) (Beauclair et al., 2015). In this case, the 'high cut-off' setting was
466 applied. The GPS-SUMO and JASSA algorithms use fundamentally different methodologies (Chang et
467 al., 2018).

468 # References and notes

469 **Ahner, A., Gong, X., and Frizzell, R.A.** (2013). Cystic fibrosis transmembrane conductance regulator
470 degradation: cross-talk between the ubiquitylation and SUMOylation pathways. FEBS Journal
471 **280,** 4430-4438.
472 **Alonso, J.M., Stepanova, A.N., Leisse, T.J., Kim, C.J., Chen, H., Shinn, P., Stevenson, D.K.,**
473 **Zimmerman, J., Barajas, P., Cheuk, R., Gadrinab, C., Heller, C., Jeske, A., Koesema, E.,**
474 **Meyers, C.C., Parker, H., Prednis, L., Ansari, Y., Choy, N., Deen, H., Geralt, M., Hazari, N.,**
475 **Hom, E., Karnes, M., Mulholland, C., Ndubaku, R., Schmidt, I., Guzman, P., Aguilar-**
476 **Henonin, L., Schmid, M., Weigel, D., Carter, D.E., Marchand, T., Risseeuw, E., Brogden, D.,**
477 **Zeko, A., Crosby, W.L., Berry, C.C., and Ecker, J.R.** (2003). Genome-wide insertional
478 mutagenesis of *Arabidopsis thaliana*. Science **301,** 653-657.
479 **Aronsson, H., Combe, J., Patel, R., Agne, B., Martin, M., Kessler, F., Jarvis, P.** (2010). Nucleotide
480 binding and dimerization at the chloroplast pre-protein import receptor, atToc33, are not
481 essential in vivo but do increase import efficiency. Plant Journal **63,** 297-311.
482 **Ayaydin, F., and Dasso, M.** (2004). Distinct in vivo dynamics of vertebrate SUMO paralogues.
483 Molecular Biology of the Cell **15,** 5208-5218.
484 **Baek, G.H., Cheng, H., Choe, V., Bao, X., Shao, J., Luo, S., and Rao, H.** (2013). Cdc48: a swiss army
485 knife of cell biology. Journal of Amino Acids **2013,** 183421.
486 **Bauer, J., Chen, K., Hiltbunner, A., Wehrli, E., Eugster, M., Schnell, D., and Kessler, F.** (2000). The
487 major protein import receptor of plastids is essential for chloroplast biogenesis. Nature **403,**
488 203-207.
489 **Beauclair, G., Bridier-Nahmias, A., Zagury, J.F., Saib, A., and Zamborlini, A.** (2015). JASSA: a
490 comprehensive tool for prediction of SUMOylation sites and SIMs. Bioinformatics **31,** 3483-
491 3491.
492 **Berardini, T.Z., Reiser, L., Li, D., Mezheritsky, Y., Muller, R., Strait, E., and Huala, E.** (2015). The
493 Arabidopsis information resource: Making and mining the "gold standard" annotated
494 reference plant genome. Genesis **53,** 474-485.
495 **Bergink, S., Ammon, T., Kern, M., Schermelleh, L., Leonhardt, H., and Jentsch, S.** (2013). Role of
496 Cdc48/p97 as a SUMO-targeted segregase curbing Rad51-Rad52 interaction. Nature Cell
497 Biology **15,** 526-532.
498 **Chang, C.C., Tung, C.H., Chen, C.W., Tu, C.H., and Chu, Y.W.** (2018). SUMOgo: Prediction of
499 sumoylation sites on lysines by motif screening models and the effects of various post-
500 translational modifications. Scientific Reports **8,** 15512.
501 **Citovsky, V., Lee, L.Y., Vyas, S., Glick, E., Chen, M.H., Vainstein, A., Gafni, Y., Gelvin, S.B., and Tzfira,**
502 **T.** (2006). Subcellular localization of interacting proteins by bimolecular fluorescence
503 complementation *in planta*. Journal of Molecular Biology **362,** 1120-1131.
504 **Clough, S.J., and Bent, A.F.** (1998). Floral dip: a simplified method for *Agrobacterium*-mediated
505 transformation of *Arabidopsis thaliana*. Plant Journal **16,** 735-743.
506 **Desterro, J.M., Rodriguez, M.S., and Hay, R.T.** (1998). SUMO-1 modification of IkappaBalpha inhibits
507 NF-kappaB activation. Molecular Cell **2,** 233-239.
508 **Elrouby, N., and Coupland, G.** (2010). Proteome-wide screens for small ubiquitin-like modifier
509 (SUMO) substrates identify Arabidopsis proteins implicated in diverse biological processes.
510 Proceedings of the National Academy of Sciences of the United States of America **107,**
511 17415-17420.
512 **Flores-Pérez, Ú., and Jarvis, P.** (2017). Isolation and suborganellar fractionation of Arabidopsis
513 chloroplasts. Methods in Molecular Biology **1511,** 45-60.
514 **Grimmer, J., Helm, S., Dobritzsch, D., Hause, G., Shema, G., Zahedi, R.P., and Baginsky, S.** (2020).
515 Mild proteasomal stress improves photosynthetic performance in Arabidopsis chloroplasts.
516 Nature Communications **11,** 1662.

517 **Hilgarth, R.S., and Sarge, K.D.** (2005). Detection of sumoylated proteins. Methods in Molecular
518 Biology **301,** 329-338.
519 **Hirsch, S., Muckel, E., Heemeyer, F., von Heijne, G., and Soll, J.** (1994). A receptor component of the
520 chloroplast protein translocation machinery. Science **266,** 1989-1992.
521 **Huang, W.H., Ling, Q.H., Bedard, J., Lilley, K., and Jarvis, P.** (2011). In vivo analyses of the roles of
522 essential Omp85-related proteins in the chloroplast outer envelope membrane. Plant
523 Physiology **157,** 147-159.
524 **Inaba, T., Alvarez-Huerta, M., Li, M., Bauer, J., Ewers, C., Kessler, F., and Schnell, D.J.** (2005).
525 Arabidopsis Tic110 is essential for the assembly and function of the protein import
526 machinery of plastids. Plant Cell **17,** 1482-1496.
527 **Ishida, T., Fujiwara, S., Miura, K., Stacey, N., Yoshimura, M., Schneider, K., Adachi, S., Minamisawa,**
528 **K., Umeda, M., and Sugimoto, K.** (2009). SUMO E3 ligase HIGH PLOIDY2 regulates endocycle
529 onset and meristem maintenance in Arabidopsis. Plant Cell **21,** 2284–2297.
530 **Jarvis, P.** (2008). Targeting of nucleus-encoded proteins to chloroplasts in plants. New Phytologist
531 **179,** 257-285.
532 **Jarvis, P., and Lopez-Juez, E.** (2013). Biogenesis and homeostasis of chloroplasts and other plastids.
533 Nature Reviews Molecular Cell Biology **14,** 787-802.
534 **Jarvis, P., Chen, L.J., Li, H.M., Pete, C.A., Fankhauser, C., and Chory, J.** (1998). An *Arabidopsis*
535 mutant defective in the plastid general protein import apparatus. Science **282,** 100-103.
536 **Karimi, M., Inze, D., and Depicker, A.** (2002). GATEWAY vectors for *Agrobacterium*-mediated plant
537 transformation. Trends in Plant Science **7,** 193-195.
538 **Karimi, M., De Meyer, B., and Hilson, P.** (2005). Modular cloning in plant cells. Trends Plant Science
539 **10,** 103-105.
540 **Kasmati, A.R., Töpel, M., Patel, R., Murtaza, G., and Jarvis, P.** (2011). Molecular and genetic
541 analyses of Tic20 homologues in *Arabidopsis thaliana* chloroplasts. Plant Journal **66,** 877-
542 889.
543 **Kessler, F., Blobel, G., Patel, H.A., and Schnell, D.J.** (1994). Identification of two GTP-binding
544 proteins in the chloroplast protein import machinery. Science **266,** 1035-1039.
545 **Kovacheva, S., Bedard, J., Patel, R., Dudley, P., Twell, D., Rios, G., Koncz, C., and Jarvis, P.** (2005). *In*
546 *vivo* studies on the roles of Tic110, Tic40 and Hsp93 during chloroplast protein import. Plant
547 Journal **41,** 412-428.
548 **Kurepa, J., Walker, J.M., Smalle, J., Gosink, M.M., Davis, S.J., Durham, T.L., Sung, D.Y., and Vierstra,**
549 **R.D.** (2003). The small ubiquitin-like modifier (SUMO) protein modification system in
550 Arabidopsis. Accumulation of SUMO1 and -2 conjugates is increased by stress. Journal of
551 Biological Chemistry **278,** 6862-6872.
552 **Lee, S., Lee, D.W., Lee, Y., Mayer, U., Stierhof, Y.D., Jurgens, G., and Hwang, I.** (2009). Heat shock
553 protein cognate 70-4 and an E3 ubiquitin ligase, CHIP, mediate plastid-destined precursor
554 degradation through the ubiquitin-26S proteasome system in *Arabidopsis*. Plant Cell **21,**
555 3984-4001.
556 **Lee, Y.J., Kim, D.H., Kim, Y.W., and Hwang, I.** (2001). Identification of a signal that distinguishes
557 between the chloroplast outer envelope membrane and the endomembrane system in vivo.
558 Plant Cell **13,** 2175-2190.
559 **Liebelt, F., and Vertegaal, A.C.** (2016). Ubiquitin-dependent and independent roles of SUMO in
560 proteostasis. American Journal of Physiology Cell Physiology **311,** C284-C296.
561 **Ling, Q., and Jarvis, P.** (2015). Regulation of chloroplast protein import by the ubiquitin E3 ligase SP1
562 is important for stress tolerance in plants. Current Biology **25,** 2527-2534.
563 **Ling, Q., Huang, W., and Jarvis, P.** (2011). Use of a SPAD-502 meter to measure leaf chlorophyll
564 concentration in Arabidopsis thaliana. Photosynthesis Research **107,** 209-214.
565 **Ling, Q., Huang, W., Baldwin, A., and Jarvis, P.** (2012). Chloroplast biogenesis is regulated by direct
566 action of the ubiquitin-proteasome system. Science **338,** 655-659.

567 **Ling, Q., Broad, W., Trösch, R., Töpel, M., Demiral Sert, T., Lymperopoulos, P., Baldwin, A., and**
568 **Jarvis, R.P.** (2019). Ubiquitin-dependent chloroplast-associated protein degradation in
569 plants. Science **363**.
570 **Liu C., Yu H., Li L.** (2019). SUMO modification of LBD30 by SIZ1 regulates secondary cell wall
571 formation in *Arabidopsis thaliana*. PLOS Genetics **15**, e1007928.
572 **Miura, K., Rus, A., Sharkhuu, A., Yokoi, S., Karthikeyan, A.S., Raghothama, K.G., Back, D., Koo, Y.D.,**
573 **Jin, J.B., Bressan, R.A., Yun, D.J., and Hasegawa, P.M.** (2005). The Arabidopsis SUMO E3
574 ligase SIZ1 controls phosphate deficiency responses. Proceedings of the National Academy of
575 Sciences of the United States of America **102,** 9734-9734.
576 **Nie, M., Aslanian, A., Prudden, J., Heideker, J., Vashisht, A.A., Wohlschlegel, J.A., Yates, J.R., and**
577 **Boddy, M.N.** (2012). Dual recruitment of Cdc48 (p97)-Ufd1-Npl4 ubiquitin-selective
578 segregase by small ubiquitin-like modifier protein (SUMO) and ubiquitin in SUMO-targeted
579 ubiquitin ligase-mediated genome stability functions. Journal of Biological Chemistry **287,**
580 29610-29619.
581 **Perry, S.E., and Keegstra, K.** (1994). Envelope membrane proteins that interact with chloroplastic
582 precursor proteins. Plant Cell **6,** 93-105.
583 **Saracco, S.A., Miller, M.J., Kurepa, J., and Vierstra, R.D.** (2007). Genetic analysis of SUMOylation in
584 Arabidopsis: conjugation of SUMO1 and SUMO2 to nuclear proteins is essential. Plant
585 Physiology **145,** 119-134.
586 **Schneider, C.A., Rasband, W.S., and Eliceiri, K.W.** (2012). NIH Image to ImageJ: 25 years of image
587 analysis. Nature Methods **9,** 671-675.
588 **Schnell, D.J., Kessler, F., and Blobel, G.** (1994). Isolation of components of the chloroplast protein
589 import machinery. Science **266,** 1007-1012.
590 **Shanmugabalaji, V., Chahtane, H., Accossato, S., Rahire, M., Gouzerh, G., Lopez-Molina, L., and**
591 **Kessler, F.** (2018). Chloroplast biogenesis controlled by DELLA-TOC159 interaction in early
592 plant development. Current Biology **28,** 2616-2623 e2615.
593 **Sowden, R.G., Watson, S.J., and Jarvis, P.** (2018). The role of chloroplasts in plant pathology. Essays
594 in Biochemistry **62,** 21-39.
595 **Sriramachandran, A.M., and Dohmen, R.J.** (2014). SUMO-targeted ubiquitin ligases. Biochimica et
596 Biophysica Acta **1843,** 75-85.
597 **Tranel, P.J., Froehlich, J., Goyal, A., and Keegstra, K.** (1995). A component of the chloroplastic
598 protein import apparatus is targeted to the outer envelope membrane via a novel pathway.
599 The EMBO Journal **14,** 2436-2446.
600 **Tzfira, T., Tian, G.W., Lacroix, B., Vyas, S., Li, J., Leitner-Dagan, Y., Krichevsky, A., Taylor, T.,**
601 **Vainstein, A., and Citovsky, V.** (2005). pSAT vectors: a modular series of plasmids for
602 autofluorescent protein tagging and expression of multiple genes in plants. Plant Molecular
603 Biology **57,** 503.
604 **van den Burg, H.A., Kini, R.K., Schuurink, R.C., and Takken, F.L.W.** (2010). *Arabidopsis* small
605 ubiquitin-like modifier paralogs have distinct functions in development and defense. Plant
606 Cell **22,** 1998-2016.
607 **Watson, S.J., Sowden, R.G., and Jarvis, P.** (2018). Abiotic stress-induced chloroplast proteome
608 remodelling: a mechanistic overview. Journal of Experimental Botany **69,** 2773-2781.
609 **Wu, F.H., Shen, S.C., Lee, L.Y., Lee, S.H., Chan, M.T., and Lin, C.S.** (2009). Tape-Arabidopsis Sandwich
610 - a simpler Arabidopsis protoplast isolation method. Plant Methods **5,** 16.
611 **Zhao, Q., Xie, Y., Zheng, Y., Jiang, S., Liu, W., Mu, W., Liu, Z., Zhao, Y., Xue, Y., and Ren, J.** (2014).
612 GPS-SUMO: a tool for the prediction of sumoylation sites and SUMO-interaction motifs.
613 Nucleic Acids Research **42,** W325-W330.

614

Acknowledgements

We are very grateful to Alistair Haslam for initiating the genetic experiments. We also thank Dr Errin Johnson and Raman Dhaliwal (Dunn School of Pathology, University of Oxford) for assistance with the electron microscopy, and Professor Jane Langdale for advice during the course of the work. We are grateful to Pedro Bota and Rita Ross for technical support. This work was supported by the Oxford Interdisciplinary Bioscience Doctoral Training Partnership (DTP), and by grants from the Biotechnology and Biological Sciences Research Council (BBSRC) (grant numbers BB/K018442/1, BB/N006372/1, BB/R016984/1 and BB/R009333/1) to RPJ.

Competing interests

The application of CHLORAD as a technology for crop improvement is covered by a patent application (no. WO2019/171091 A).

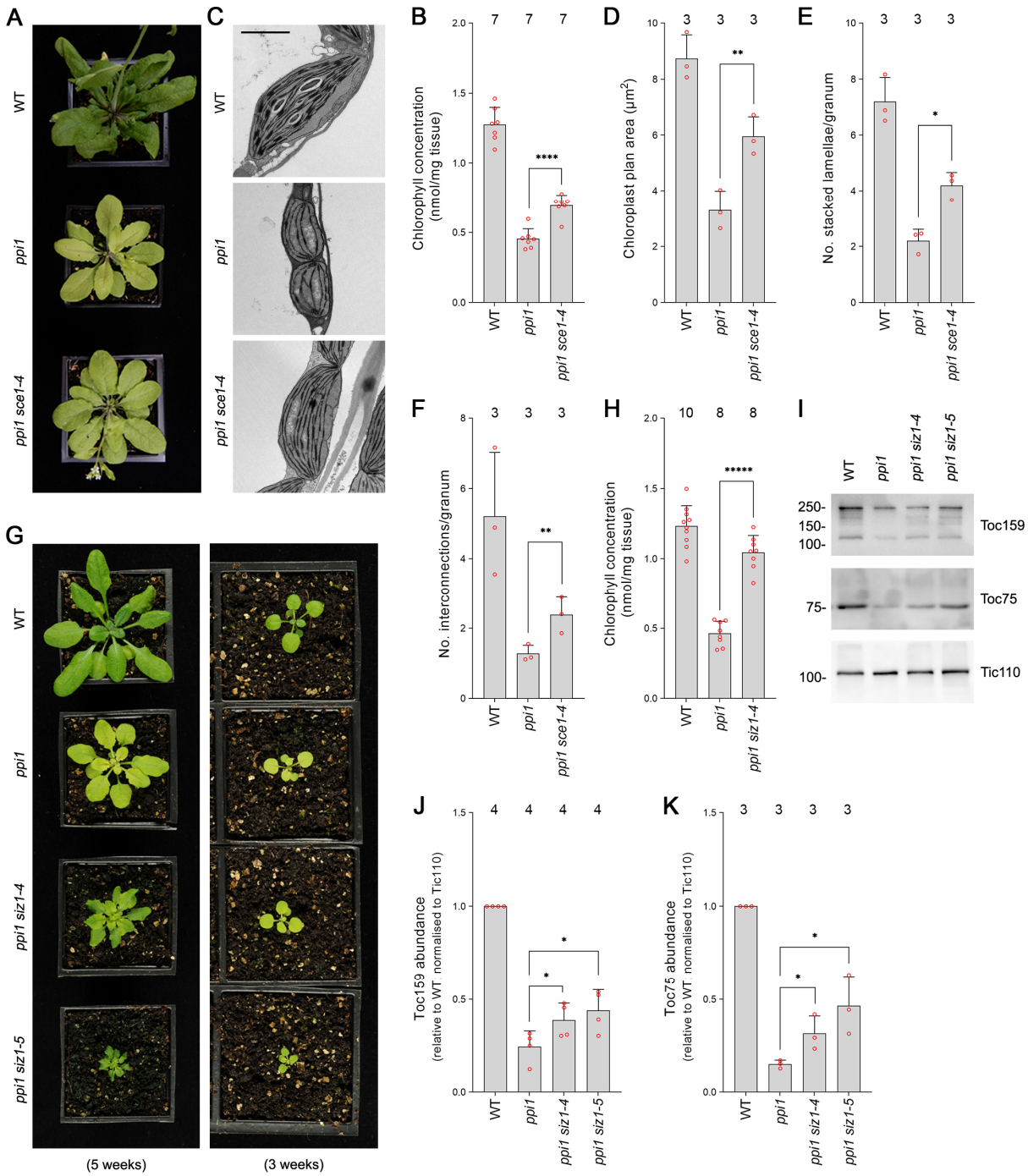

Figure 1

The E2 SUMO conjugating enzyme mutation, *sce1-4*, and the E3 SUMO ligase mutations, *siz1-4* and *siz1-5*, suppress the phenotype of plastid protein import mutant, *ppi1*.

(A) The *ppi1 sce1-4* double mutant appeared greener than *ppi1* after approximately five weeks of growth on soil. **(B)** The *ppi1 sce1-4* double mutant showed enhanced accumulation of chlorophyll relative to *ppi1* after approximately five weeks of growth on soil. Measurements were taken from the plants shown in (A) on the day of photography, as well as additional similar plants. There were significant differences between the *ppi1* and *ppi1 sce1-4* plants (Two-tailed t-test, unpaired samples, T = 6.15, p = 0.000049). **(C)** Transmission electron microscopy revealed improved chloroplast development in mature rosette leaf mesophyll tissue of *ppi1 sce1-4* plants relative to *ppi1*. Plants

638 that had been grown on soil for approximately four weeks were analysed, and representative images
639 are shown. Scale bar = 2 µm. **(D)** Chloroplast plan area was elevated in *ppi1 sce1-4* relative to *ppi1*.
640 The transmission electron microscopy dataset was quantified. There were significant differences
641 between the *ppi1* and *ppi1 sce1-4* plants (Two-tailed t-test, unpaired samples, T = 4.65, *p* =
642 0.009674). **(E, F)** Thylakoid membrane development was increased in *ppi1 sce1-4* relative to *ppi1*.
643 The number of stacked thylakoidal lamellae per granum (E), and the number of stromal thylakoidal
644 lamellae emanating from each granum (granal interconnections) (F), was analysed using the
645 transmission electron microscopy dataset. There were significant differences between the *ppi1* and
646 *ppi1 sce1-4* plants (Two-tailed t-test, unpaired samples: T = 5.53, *p* = 0.005221 [E]; T = 3.38, *p* =
647 0.0277 [F]). **(G)** The *ppi1 siz1-4* and *ppi1 siz1-5* double mutants appeared greener than *ppi1* after
648 different periods of growth on soil. The plants were photographed after three weeks of growth (right
649 panel) and then again after five weeks of growth (left panel). **(H)** The *ppi1 siz1-4* double mutant
650 showed enhanced accumulation of chlorophyll relative to *ppi1* after approximately five weeks of
651 growth on soil. Measurements were taken from the plants shown in (G) on the day of photography,
652 as well as additional similar plants. There were significant differences between the *ppi1* and *ppi1*
653 *siz1-4* plants (Two-tailed t-test, unpaired samples, T = 11.01, *p* < 0.00001). **(I)** TOC protein
654 accumulation was improved in *ppi1 siz1-4* and *ppi1 siz1-5* relative to *ppi1*. Analysis of the levels of
655 Toc75 and Toc159 in *ppi1 siz1-4*, *ppi1 siz1-5*, and relevant control plants was conducted by
656 immunoblotting. Protein samples were taken from whole seedlings that had been grown on soil for
657 approximately two weeks (the plants shown in Figure 1 – Supplement 1C on the day of
658 photography). Tic110, a TIC-associated protein, was included as a compartment-specific loading
659 control. Migration positions of standards are displayed to the left of the gel images, and sizes are
660 indicated in kDa. Unprocessed membrane images are displayed in Source data 1. **(J, K)** Toc159 and
661 Toc75 protein accumulation was improved in *ppi1 siz1-4* and *ppi1 siz1-5* relative to *ppi1*. Specific
662 bands in (I) and in Source data 1 were quantified. Error bars indicate standard deviation from the
663 mean. The numbers above the graph indicate the number of biological replicates per sample. There
664 were significant differences between the *ppi1* and *ppi1 siz1-4* samples (One-tailed t-test, unpaired
665 samples: T = 2.26, *p* = 0.032316 [J, Toc159]; T = 2.93, *p* = 0.021334 [K, Toc75]) and between the *ppi1*
666 and *ppi1 siz1-5* samples (One-tailed t-test, unpaired samples: T = 2.76, *p* = 0.01639 [J, Toc159]; T =
667 3.36, *p* = 0.014118 [K, Toc75]). In all bar charts, error bars indicate standard deviation from the
668 mean, and open red circles indicate individual data points. The numbers above the graphs indicate
669 the number of biological replicates per sample. Statistical significance is indicated as follows: *,
670 *p*<0.05; **, *p*<0.01; ****, *p*<0.0001; *****, *p*<0.00001.

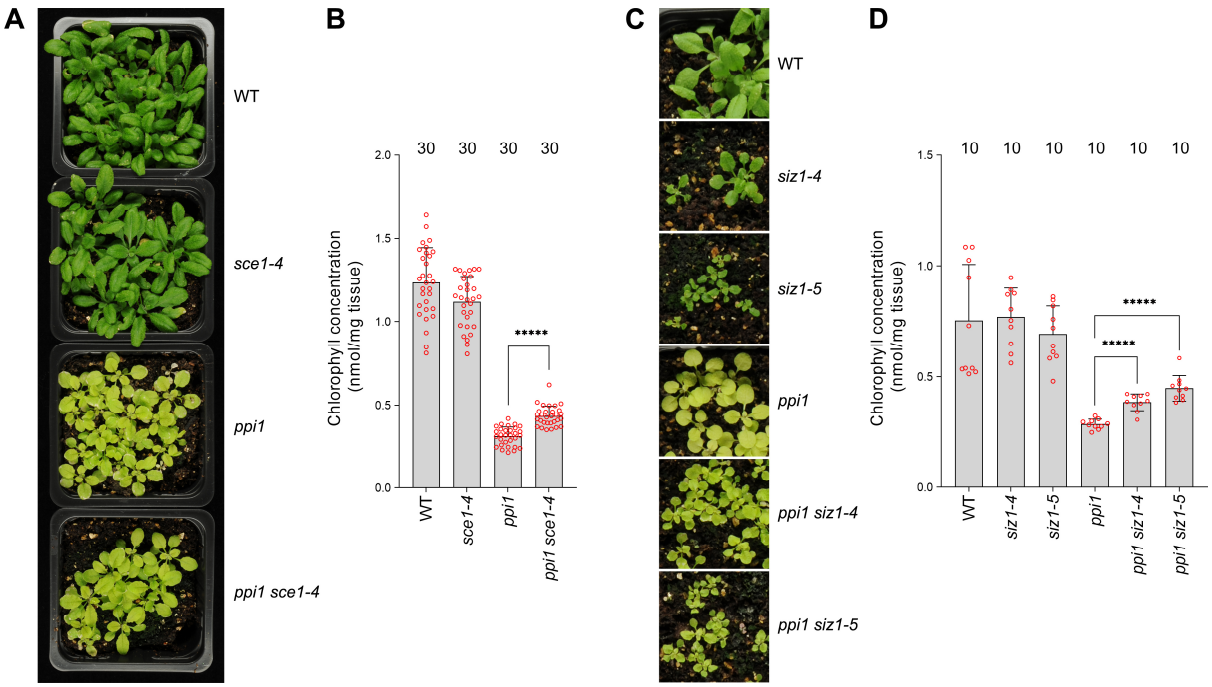

Figure 1 – Supplement 1

The E2 SUMO conjugating enzyme mutation, *sce1-4*, and the E3 SUMO ligase mutations, *siz1-4* and *siz1-5*, suppress the phenotype of plastid protein import mutant, *ppi1*.

(A) The *ppi1 sce1-4* double mutant appeared greener than *ppi1* after approximately three weeks of growth on soil, while the single *sce1-4* mutant appeared no greener than the wild-type control. **(B)** The *ppi1 sce1-4* double mutant showed enhanced accumulation of chlorophyll relative to *ppi1* after approximately three weeks of growth on soil (T = 8.19, $p < 0.0001$), while the single *sce1-4* mutant displayed no enhanced accumulation of chlorophyll relative to the wild-type control. Measurements were taken from the plants shown in (A) on the day of photography, as well as additional similar plants. **(C)** The *ppi1 siz1-4* and *ppi1 siz1-5* double mutants appeared greener than *ppi1* after approximately two weeks of growth on soil, while the single *siz1-4* and *siz1-5* mutants appeared no greener than the wild-type control. **(D)** The *ppi1 siz1-4* and *ppi1 siz1-5* double mutants showed enhanced accumulation of chlorophyll relative to *ppi1* after approximately two weeks of growth on soil (T = 7.16, $p < 0.0001$ and T = 8.26, $p < 0.0001$ respectively), while the single *siz1-4* and *siz1-5* mutants displayed no enhanced accumulation of chlorophyll relative to the wild-type control. Measurements were taken from the plants shown in (C) on the day of photography, as well as additional similar plants. In all bar charts, error bars indicate standard deviation from the mean, and open red circles indicate individual data points. The numbers above the graphs indicate the number of biological replicates per sample. Statistical significance is indicated as follows: *****, $p<0.00001$.

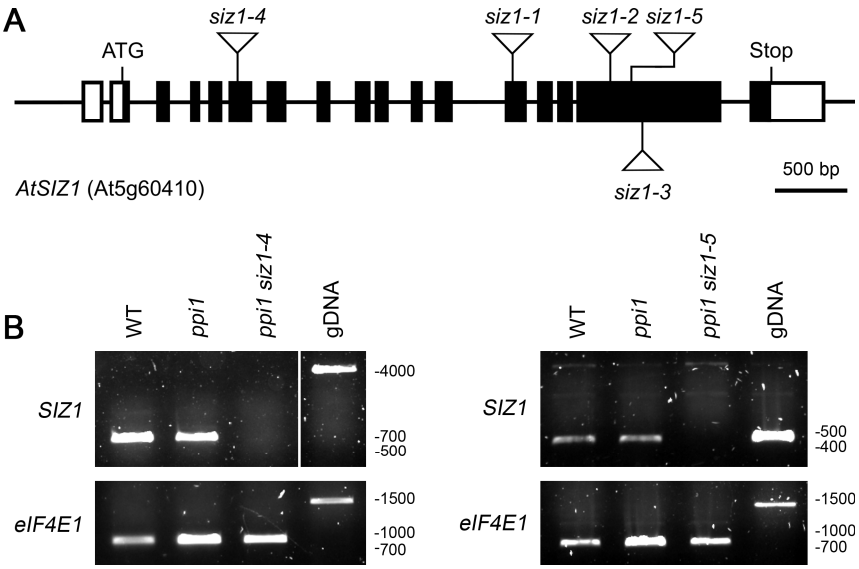

693

694

695 **Figure 1 – Supplement 2**

696 **Molecular analysis of the *siz1-4* and *siz1-5* mutants.**

697 **(A)** Schematic representation of the *SIZ1* (At5g60410) gene, annotated with the positions of the *siz1*
698 T-DNA insertions. The *siz1-4* and *siz1-5* insertion sites were verified in this study by DNA sequencing.
699 The black boxes indicate exons, while the interconnecting black lines represent introns. The white
700 boxes indicate untranslated regions. **(B)** Analysis of *SIZ1* mRNA expression in *siz1-4* and *siz1-5*. RNA
701 samples were taken from two-week-old seedlings and used as a template for cDNA synthesis.
702 Primers specific to *SIZ1* and the reference gene *eIF4E1* were used in two parallel RT-PCR
703 experiments. gDNA, genomic DNA. Migration positions of standards are displayed to the right of the
704 gel images, and sizes are indicated in base pairs.

705

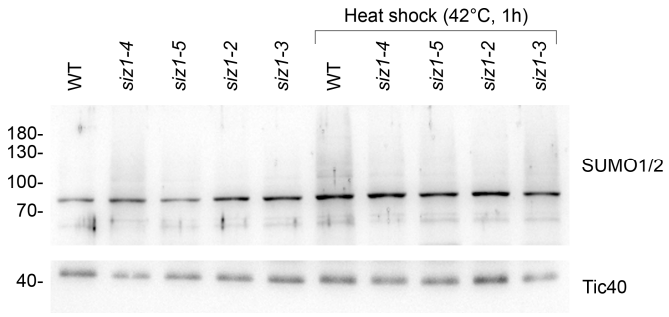

706

707 **Figure 1 – Supplement 3**

708 **The *siz1-4* and *siz1-5* mutants display reduced global SUMOylation in response to heat shock.**

709 14-day-old seedlings of the indicated genotypes were subjected to heat shock (42°C for 1 hour,
710 followed by a 1-hour recovery period at 22°C). Protein samples were taken from whole seedlings and
711 analysed by immunoblotting. The *siz1-4* and *siz1-5* mutants displayed a moderate reduction of global
712 SUMOylation, and this reduction was similar in magnitude to the reduction observed in the
713 previously characterised *siz1-2* and *siz1-3* mutants. The unprocessed membrane images are
714 displayed in Source data 1.

715

716

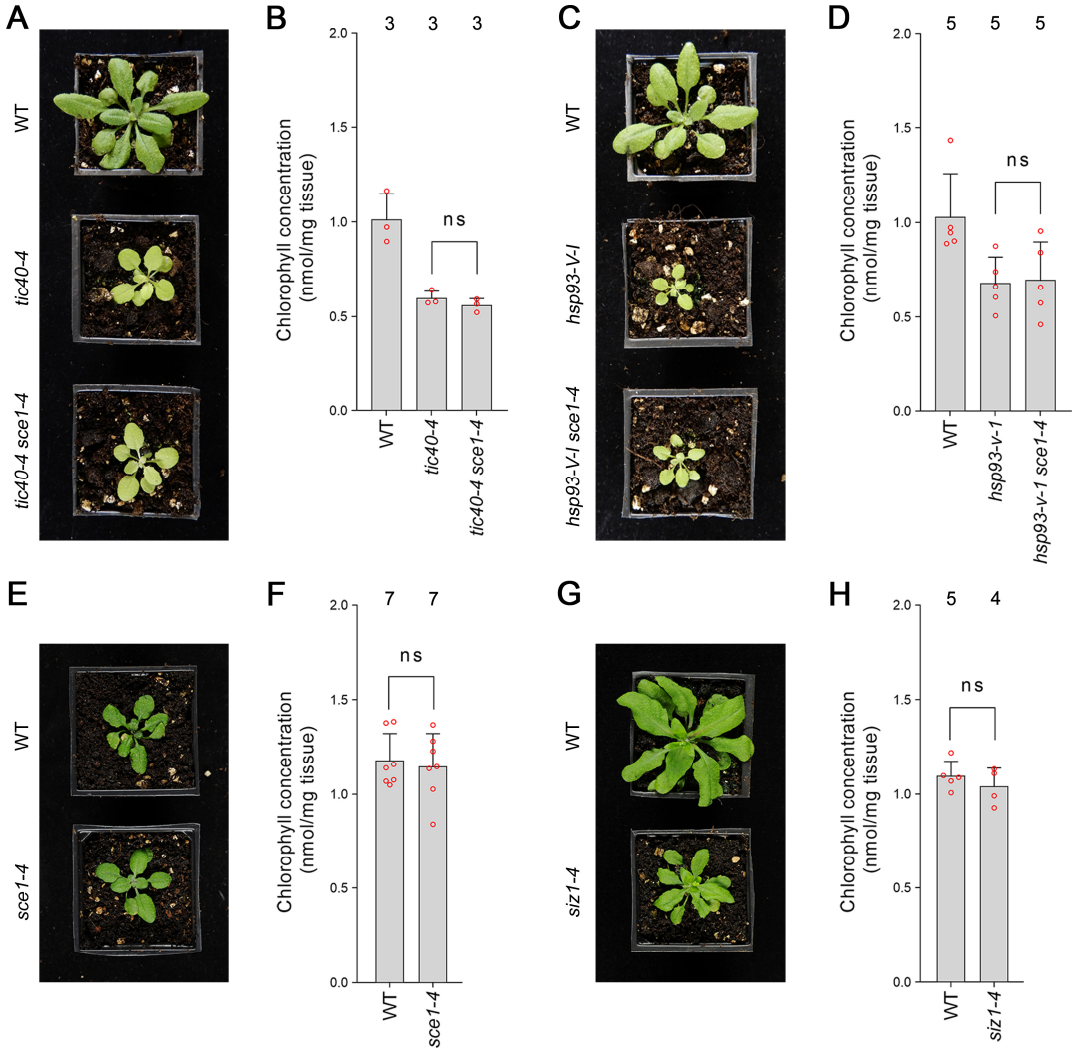

717

718 **Figure 2**

719 **Genetic analysis reveals specificity of the suppression mediated by the *sce1-4* and *siz1-4***
720 **mutations.**

721 **(A)** The *tic40-4 sce1-4* double mutant did not appear greener than *tic40-4* after approximately four
722 weeks of growth on soil. **(B)** The *tic40-4 sce1-4* double mutant did not show an enhanced
723 accumulation of chlorophyll relative to *tic40-4* after approximately four weeks of growth on soil.
724 Measurements were taken from the plants shown in (A) on the day of photography, as well as
725 additional similar plants. There were no significant differences between the *tic40-4* and *tic40-4 sce1-*
726 *4* plants (Two-tailed t-test, unpaired samples, T = 1.25, p = 0.280106). **(C)** The *hsp93-V-1 sce1-4*
727 double mutant did not appear greener than *hsp93-V-1* after approximately four weeks of growth on
728 soil. **(D)** The *hsp93-V-1 sce1-4* double mutant did not show an enhanced accumulation of chlorophyll
729 relative to *hsp93-V-1* after approximately four weeks of growth on soil. Measurements were taken
730 from the plants shown in (C) on the day of photography, as well as additional similar plants. There
731 were no significant differences between the *hsp93-V-1* and *hsp93-V-1 sce1-4* plants (Two-tailed t-
732 test, unpaired samples, T = 0.18, p = 0.860702). **(E)** The *sce1-4* single mutant did not appear greener
733 than wild-type plants after approximately four weeks of growth on soil. **(F)** The *sce1-4* single mutant
734 did not show an enhanced accumulation of chlorophyll relative to wild-type plants after

approximately four weeks of growth on soil. Measurements were taken from the plants shown in (E) on the day of photography, as well as additional similar plants. There were no significant differences between the *sce1-4* and wild type plants (Two-tailed t-test, unpaired samples, T = 0.38, p = 0.708484). **(G)** The *siz1-4* single mutant did not appear greener than wild-type plants after approximately five weeks of growth on soil. **(H)** The *siz1-4* single mutant did not show an enhanced accumulation of chlorophyll relative to wild-type plants after approximately five weeks of growth on soil. Measurements were taken from the plants shown in (G) on the day of photography, as well as from additional similar plants. There were no significant differences between the *siz1-4* and wild type plants (T = 0.96, p = 0.370055). In all bar charts, error bars indicate standard deviation from the mean, and open red circles indicate individual data points. The numbers above the graphs indicate the number of biological replicates per sample. Statistical significance is indicated as follows: ns, not significant.

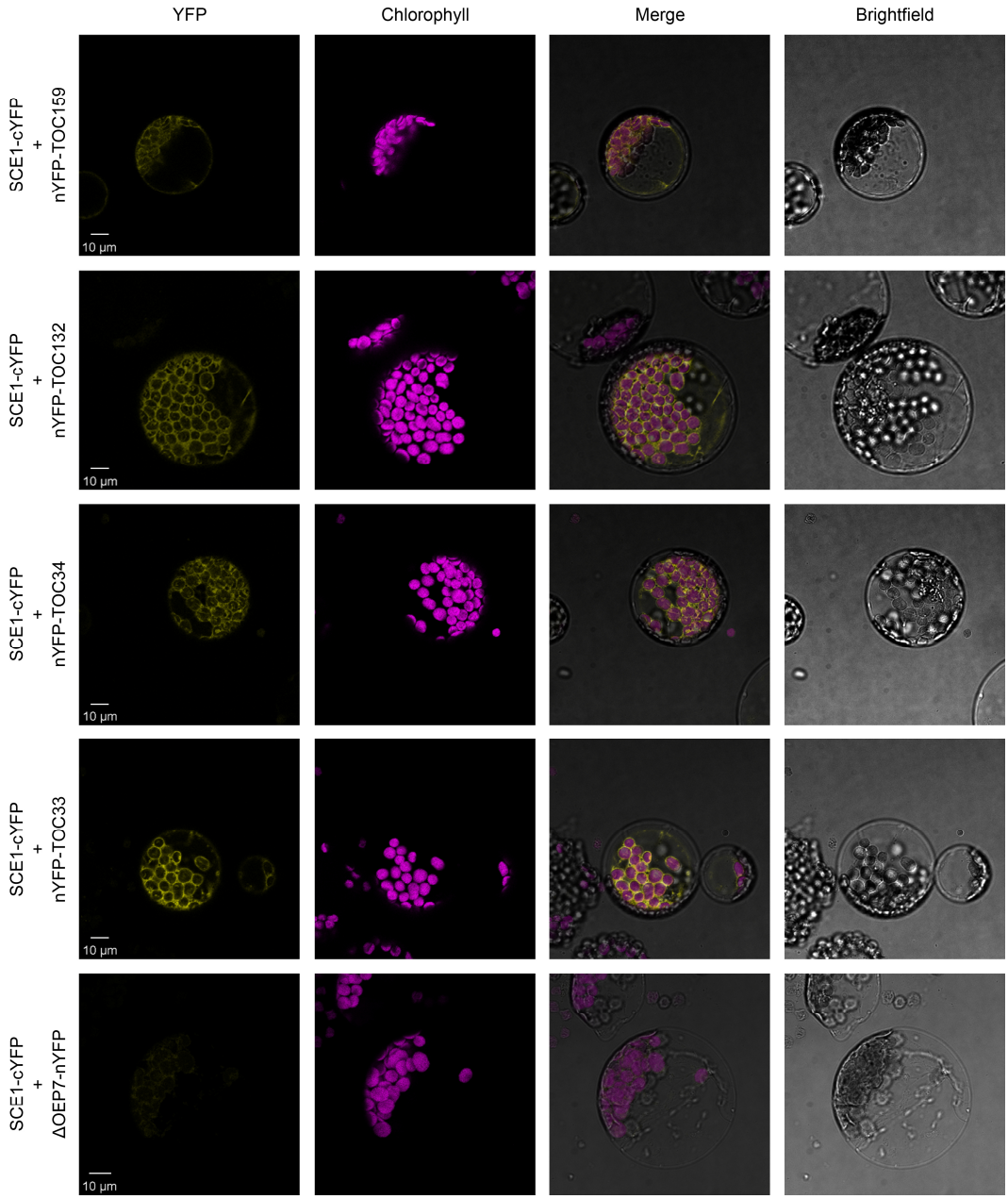

Figure 3

SCE1 physically interacts with TOC proteins *in vivo.*

Bimolecular fluorescence complementation (BiFC) analysis of SCE1 protein-protein interactions was performed by imaging *Arabidopsis* protoplasts co-expressing proteins fused to complementary N-terminal (nYFP) and C-terminal (cYFP) fragments of the YFP protein, as indicated. Chlorophyll autofluorescence images were used to orientate the YFP signals in relation to the chloroplasts. SCE1 physically associated with all tested TOC proteins. The images shown are representative confocal micrographs indicating associations between SCE1 and Toc159, Toc132, Toc34 and Toc33. In contrast, SCE1 did not physically associate with ΔOEP7 (comprising the transmembrane domain of OEP7, which is sufficient to direct targeting to the chloroplast outer envelope), which served as a negative control. Scale bars = 10 µm.

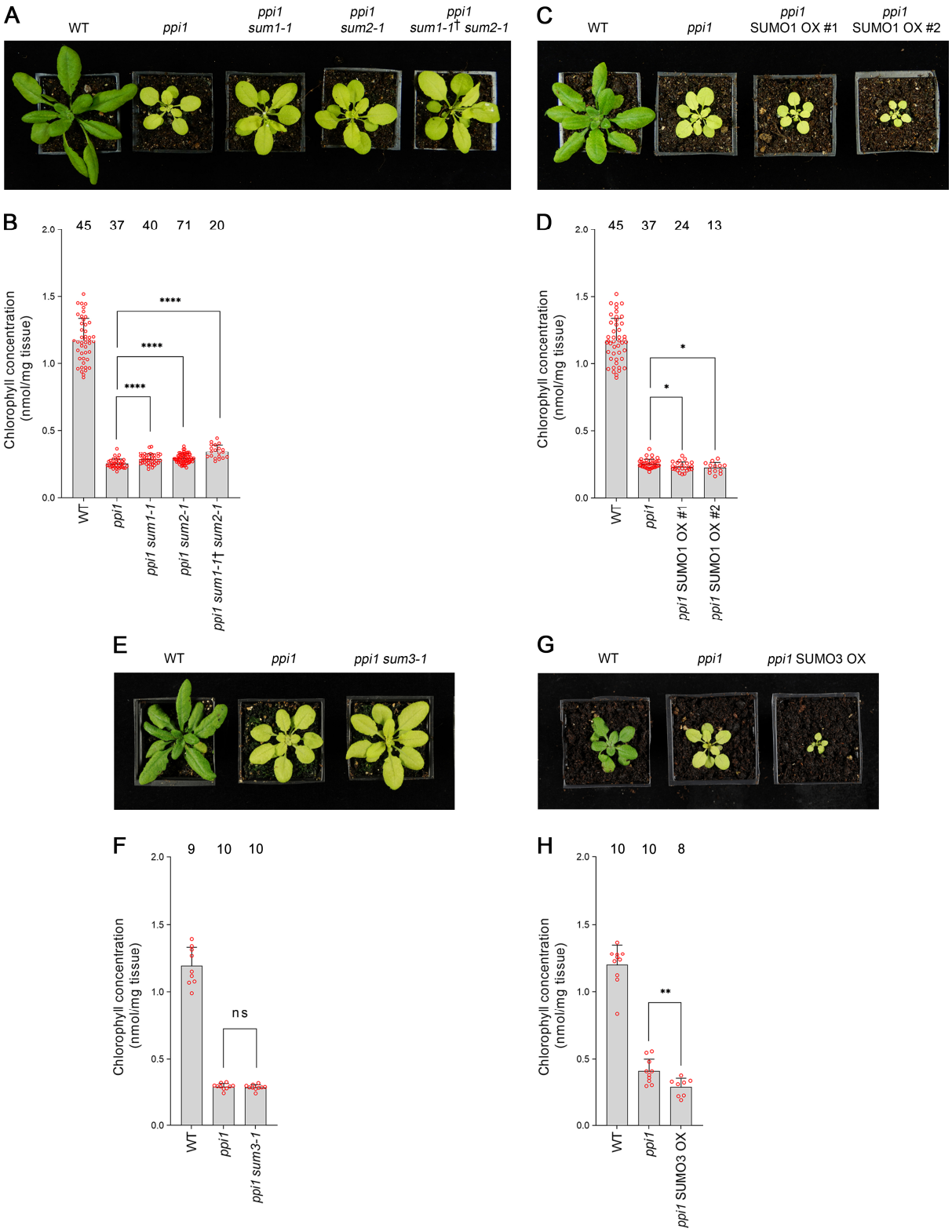

Figure 4

Genetic interactions between *ppi1* and the genes encoding three SUMO isoforms.

(A) The *ppi1 sum1-1*, *ppi1 sum2-1*, and *ppi1 sum1-1*† *sum2-1* double and triple mutants appeared greener than *ppi1* after approximately four weeks of growth on soil. The dagger symbol indicates that the triple mutant was heterozygous with respect to the *sum1-1* mutation. **(B)** The *ppi1 sum1-1*, *ppi1 sum2-1*, and *ppi1 sum1-1*† *sum2-1* double and triple mutants showed enhanced accumulation

of chlorophyll relative to *ppi1* after approximately four weeks of growth on soil. Measurements were taken from the plants shown in (A) on the day of photography, as well as additional similar plants. There were significant differences between the samples, as measured via a one-way ANOVA ($F = 26.21$, $p = 6.65 \times 10\text{-}14$). A post-hoc Tukey HSD test indicated that there was a significant difference between the *ppi1* and *ppi1 sum1-1* samples ($p < 0.00001$). There were also significant differences between the *ppi1* and *ppi1 sum2-1* samples ($p < 0.00001$), and between the *ppi1* and *ppi1 sum1-1*† *sum2-1* samples ($p < 0.00001$). **(C)** The *ppi1* SUMO1 overexpression (OX) lines appeared smaller and paler than *ppi1* after approximately four weeks of growth on soil. **(D)** The *ppi1* SUMO1 OX lines showed reduced accumulation of chlorophyll relative to *ppi1* after approximately four weeks of growth on soil. Measurements were taken from the plants shown in (C) on the day of photography, as well as additional similar plants. There were significant differences between the *ppi1* and *ppi1* SUMO1 OX #1 plants (Two-tailed t-test, unpaired samples, $T = 2.27$, $p = 0.026832$), and between the *ppi1* and *ppi1* SUMO1 OX #2 plants (Two-tailed t-test, unpaired samples, $T = 2.49$, $p = 0.01634$). **(E)** The *ppi1 sum3-1* double mutant did not appear greener than *ppi1* after approximately four weeks of growth on soil. **(F)** The *ppi1 sum3-1* double mutant did not show an enhanced accumulation of chlorophyll relative to *ppi1* after approximately four weeks of growth on soil. Measurements were taken from the plants shown in (E) on the day of photography, as well as additional similar plants. There were no significant differences between the *ppi1* and *ppi1 sum3-1* plants (Two-tailed t-test, unpaired samples, $T = 0.54$, $p = 0.59407$). **(G)** The *ppi1* SUMO3 overexpression line appeared smaller and paler than *ppi1* after approximately three weeks of growth on soil. **(H)** The *ppi1* SUMO3 overexpression line showed reduced accumulation of chlorophyll relative to *ppi1* after approximately three weeks of growth on soil. Measurements were taken from the plants shown in (G) on the day of photography, as well as additional similar plants. There were significant differences between the *ppi1* SUMO3 OX plants and *ppi1* (Two-tailed t-test, unpaired samples, $T = 2.99$, $p = 0.008688$). In all bar charts, error bars indicate standard deviation from the mean, and open red circles indicate individual data points. The numbers above the graphs indicate the number of biological replicates per sample. Statistical significance is indicated as follows: ns, not significant; *, $p<0.05$; **, $p<0.01$; ****, $p<0.0001$.

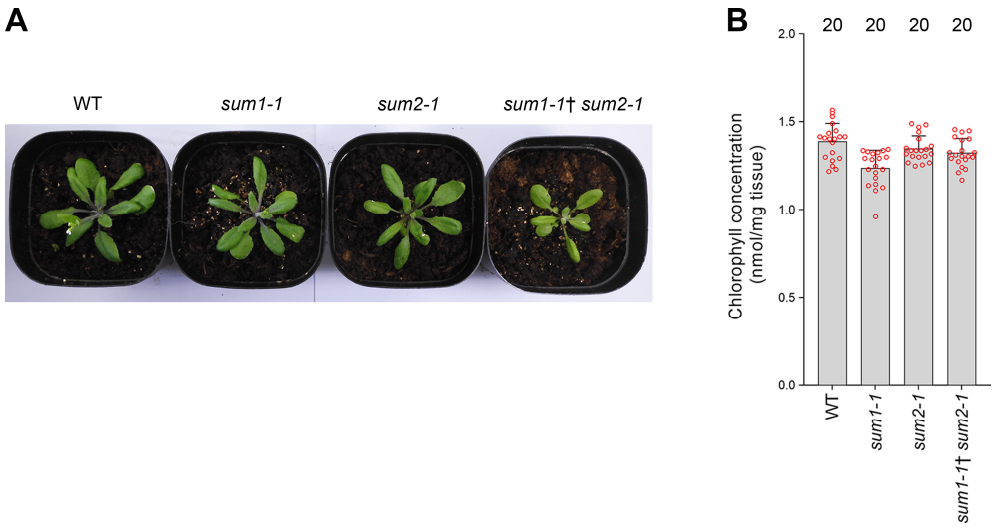

Figure 4 – Supplement 1

The *sum1-1*, *sum2-1*, and *sum1-1*† *sum2-1* single and double mutants do not show enhanced chlorophyll accumulation relative to wild-type plants.

(A) The *sum1-1*, *sum2-1*, and *sum1-1*† *sum2-1* mutants did not appear greener than wild-type plants after approximately four weeks of growth on soil. **(B)** The *sum1-1*, *sum2-1*, and *sum1-1*† *sum2-1* mutants did not show enhanced chlorophyll accumulation relative to wild-type plants after approximately four weeks of growth on soil. The dagger symbol indicates that the double mutant was heterozygous with respect to the *sum1-1* mutation. Error bars indicate standard deviation from the mean, and open red circles indicate individual data points. The numbers above the graph indicate the number of biological replicates per sample.

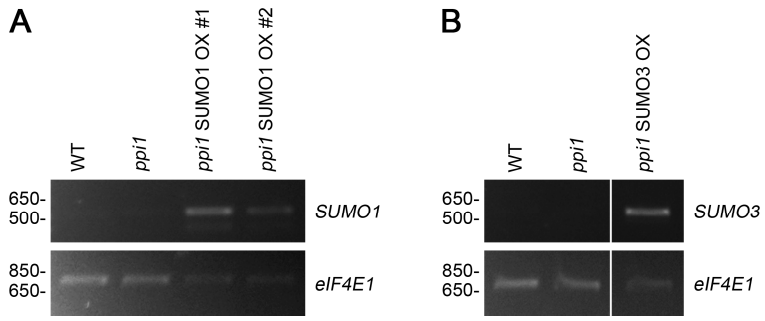

Figure 4 – Supplement 2

Analysis of the expression of the 35S:*SUMO1* and 35S:*SUMO3* transgenes in the selected transformants by RT-PCR.

Total RNA was extracted from the rosette tissue of plants that had been grown on soil for approximately four weeks. The expression of *SUMO1* **(A)** or *SUMO3* **(B)**, and of the control gene, *eIF4E1*, was analysed by semi-quantitative RT-PCR. A limited number of amplification cycles (n = 26) were employed to prevent saturation. Migration positions of standards are displayed to the left of the gel images, and sizes are indicated in base pairs.

822

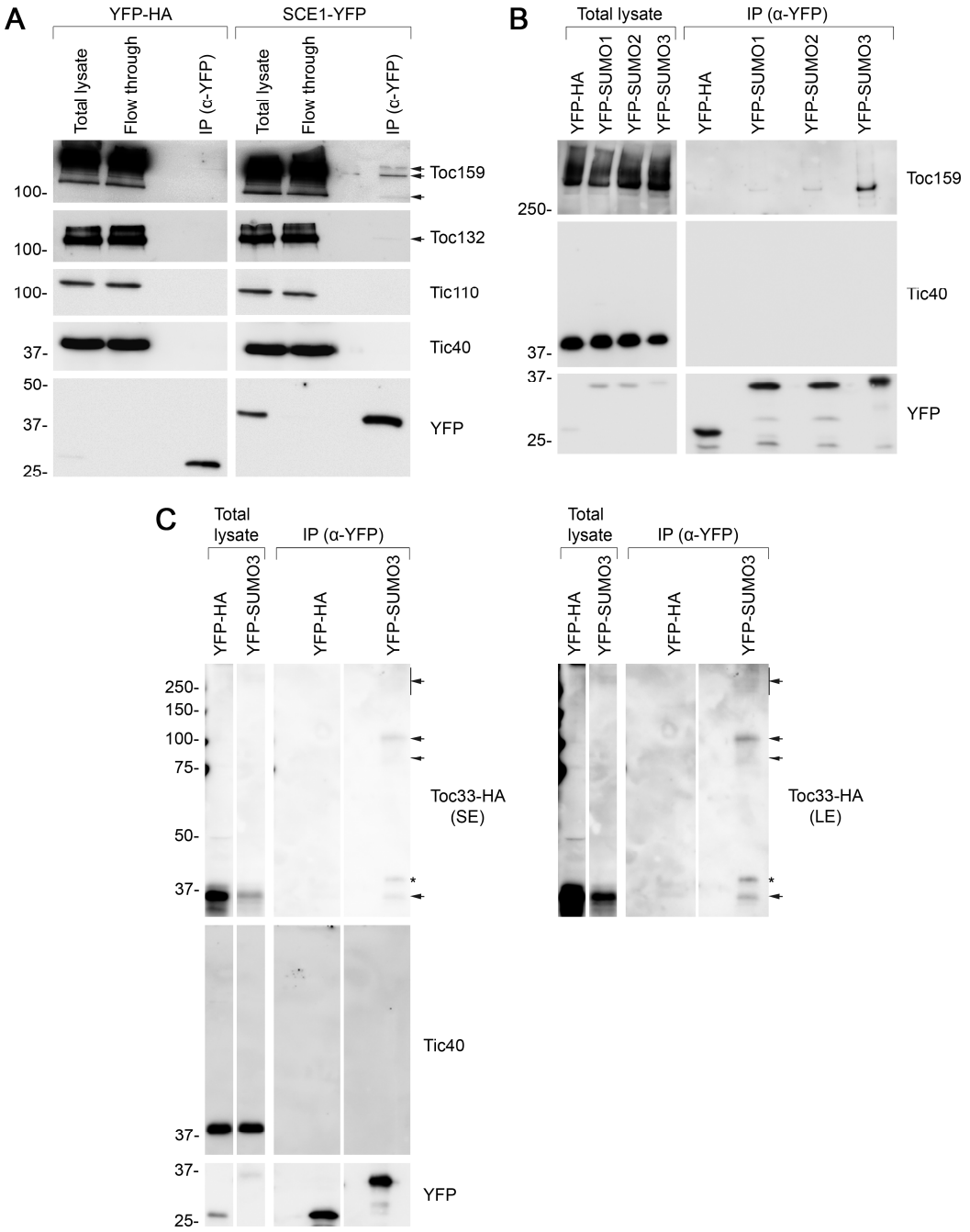

823

824

825 **Figure 5**

826 **Immunoprecipitation analysis reveals that TOC proteins are SUMO targets.**

827 **(A)** SCE1 physically associated with native TOC proteins. *Arabidopsis* protoplasts expressing YFP-HA
828 (left panel) or SCE1-YFP (right panel) were solubilised and subjected to immunoprecipitation (IP)
829 analysis. The YFP-HA construct served as a negative control. In both cases, three samples were
830 analysed: The 'Total lysate' sample (total protein extract from solubilised protoplasts); the 'Flow
831 through' sample (the total protein sample after incubation with anti-YFP beads); and the 'IP' sample
832 (the eluted fraction of the total protein sample that bound to the anti-YFP beads). The samples were
833 analysed by immunoblotting, revealing that SCE1-YFP, but not the YFP-HA control, was associated

834 with native Toc159 and Toc132 (indicated by the two arrows). Neither SCE1-YFP nor YFP-HA was
835 associated with native Tic110 or Tic40, which were included as negative control proteins. **(B)** All
836 three SUMO isoforms physically associated with native Toc159. Protoplasts expressing YFP-HA, YFP-
837 SUMO1, YFP-SUMO2 or YFP-SUMO3 were solubilised and subjected to IP analysis as in (A). In all four
838 cases, two samples (the 'Total lysate' and the 'IP' samples) were analysed by immunoblotting.
839 Toc159 was resolved on an 8% acrylamide gel for four hours to maximise the resolution of high
840 molecular weight bands. All three YFP-SUMO proteins were found to associate with native Toc159;
841 however, YFP-SUMO3 immunoprecipitated Toc159 with the greatest efficiency. None of the four YFP
842 fusion proteins associated with native Tic40, which served as a negative control protein. **(C)** YFP-
843 SUMO3 physically associated with Toc33-HA and related high molecular weight species. Protoplasts
844 co-expressing YFP-SUMO3 or YFP-HA together with Toc33-HA were solubilised and subjected to IP
845 analysis as in (A). In both cases, two samples (the 'Total lysate' and 'IP' samples) were analysed by
846 immunoblotting. The results showed that YFP-SUMO3, but not YFP-HA, was associated with Toc33-
847 HA (indicated by the arrow). Bands corresponding to the molecular weight of Toc33-HA bearing one,
848 two or several YFP-SUMO3 motifs were detected on the membrane (indicated by the upper arrows).
849 The predicted molecular weight of YFP-SUMO3 is approximately 38.9 kDa. Neither YFP-SUMO3 nor
850 YFP-HA was associated with Tic40, which served as a negative control protein. The asterisk indicates
851 a nonspecific band. Short (SE) and long (LE) exposures are shown. Migration positions of standards
852 are displayed to the left of the gel images, and sizes are indicated in kDa. The unprocessed
853 membrane images are displayed in Source data 1.
854

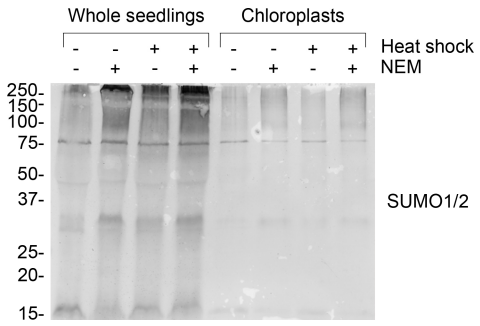

855

856

857 **Figure 5 – Supplement 1**

858 **Chloroplast resident proteins are SUMOylated.**

859 Anti-SUMO1 immunoblot of protein samples taken from whole seedlings (left hand side) and
860 isolated chloroplasts (right hand side). Where indicated, seedlings were exposed to heat shock (42°C
861 for one hour) and/or incubated with 10 mM N-ethylmaleimide (NEM) to aid the detection of
862 SUMOylated proteins. The anti-SUMO1 antibody shows significant cross-reactivity with SUMO2.
863 Migration positions of standards are displayed to the left of the gel images, and sizes are indicated in
864 kDa.

865

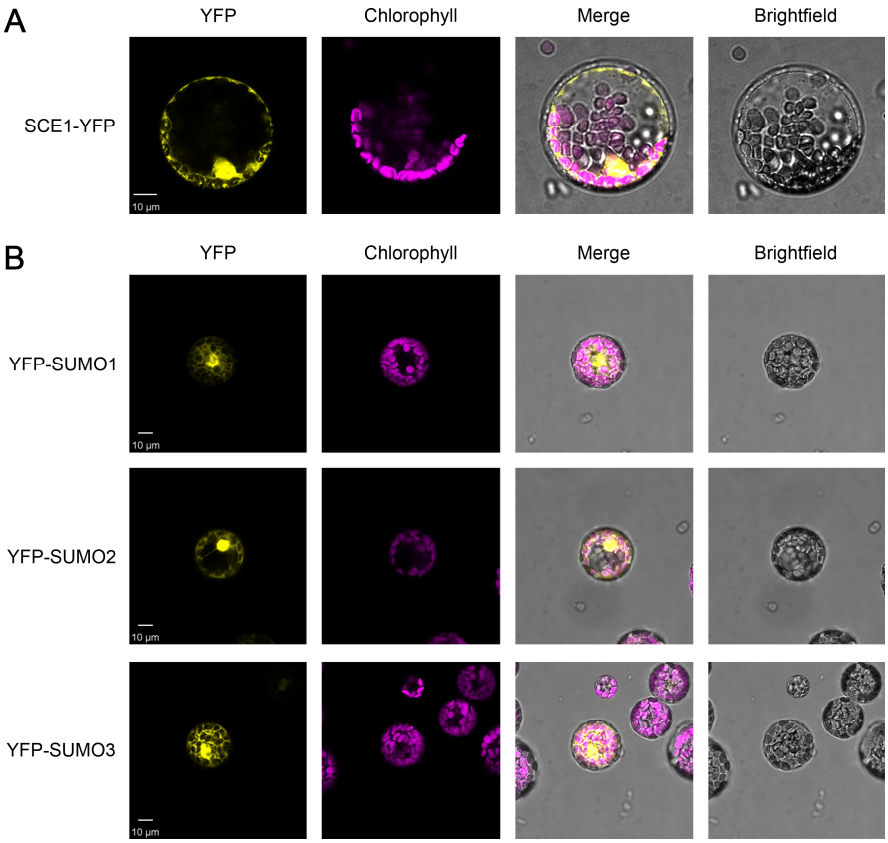

Figure 5 – Supplement 2

Analysis of the expression of the YFP-tagged constructs used in the immunoprecipitation experiments by confocal microscopy.

The expression of the SCE1-YFP construct **(A)**, and of the three YFP-SUMO constructs **(B)**, was analysed and confirmed by imaging transfected *Arabidopsis* protoplasts. Chlorophyll autofluorescence images were employed to orientate the YFP signals in relation to the chloroplasts. Representative confocal micrographs show a typical protoplast in each case. Scale bars = 10 µm.

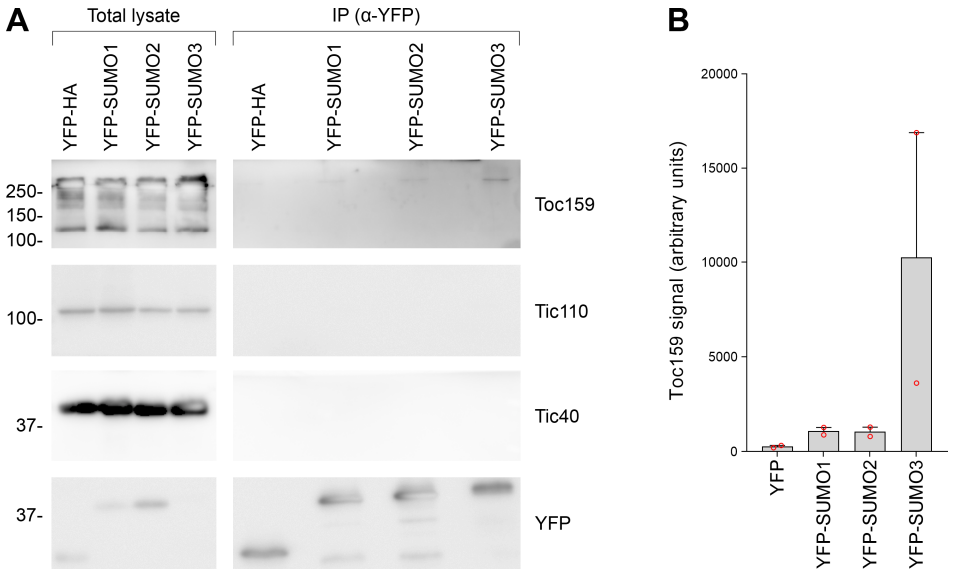

Figure 5 – Supplement 3

All three SUMO isoforms physically associated with native Toc159, with SUMO3 showing the strongest association.

(A) The immunoprecipitation experiment shown in Figure 5B was repeated. Tic110 was included as an additional negative control. The samples were run on a 10% acrylamide gel for 1 hour, as opposed to an 8% acrylamide gel for four hours (as in Figure 5B). Migration positions of standards are displayed to the left of the gel images, and sizes are indicated in kDa. The unprocessed membrane images are displayed in Source data 1. **(B)** The Toc159 bands in the eluted fractions in the two experiments, in (A) and in Figure 5B, were quantified. Error bars indicate standard deviation from the mean, and open red circles indicate individual data points.

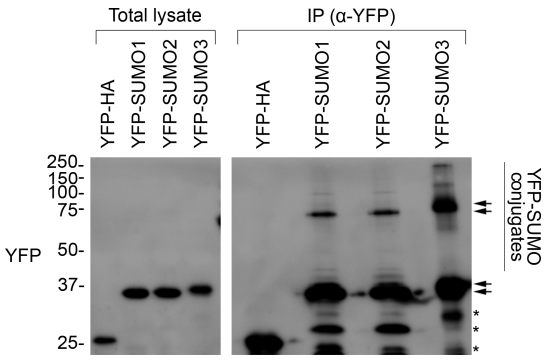

Figure 5 – Supplement 4

All three YFP-SUMO probes are conjugation-competent.

The membrane shown is the same as the one presented in Figure 5B (YFP panel). In this case, the membrane was visualised using a long exposure to aid the detection of weakly abundant protein bands. As well as the YFP-SUMO monomers, additional high molecular bands and smears were seen in the IP samples, indicating the capture of large numbers of SUMOylated proteins. This shows that all three YFP-SUMO probes could be successfully conjugated, as expected (Ayaydin and Dasso, 2004). The positions of the YFP-SUMO monomers (lower pair of arrows), and of the various SUMO adducts (vertical bar) potentially including di-SUMO (upper pair of arrows), are indicated. Note that YFP-SUMO3 migrated more slowly than the other two fusions, as expected. The asterisks indicate non-specific bands. Migration positions of standards are displayed to the left of the gel images, and sizes are indicated in kDa.

904 **Table 1**

905 **Bioinformatic analysis predicts that the core TOC proteins in *Arabidopsis* contain SUMOylation**
906 **sites and SUMO interaction motifs.**

907 The GPS-SUMO algorithm was applied to the amino acid sequences of Toc159, Toc132, Toc120,
908 Toc90, Toc75, Toc33 and Toc34 using the 'high stringency' setting, and the results generated are
909 shown in columns 2, 3 and 4. 'Consensus' sites fall within canonical SUMO site motifs: ψ-K-X-E
910 (where ψ indicates a hydrophobic amino acid, and X indicates any amino acid residue). 'Non-
911 consensus' sites do not fall within canonical SUMO site motifs; analysis shows that ~40% of
912 SUMOylation may occur at non-consensus sites (Zhao et al., 2014). 'SUMO Interaction' sites are
913 predicted to mediate the non-covalent interaction between proteins and SUMO peptides. The JASSA
914 algorithm was also applied to the amino acid sequences using the 'high cut-off' setting (see column
915 5). aa denotes amino acids.

916

Protein name	Position (aa)	*p*-value	Type	Also predicted by JASSA (high stringency)?
atToc159	95	0.021	Consensus	No
(At4g02510)	106	0.034	Consensus	Yes
1503 aa	126	0.032	Consensus	Yes
	144	0.02	Consensus	Yes
	151	0.02	Consensus	No
	246-250	0.005	SUMO Interaction	Yes
	408-412	0.009	SUMO Interaction	Yes
	486-490	0.009	SUMO Interaction	Yes
	498	0.022	Consensus	No
	502	0.049	Non-consensus	No
	539	0.026	Consensus	No
	1300	0.049	Non-consensus	No
	1370	0.01	Consensus	Yes
atToc132	30	0.006	Consensus	Yes
(At2g16640)	66	0.036	Consensus	Yes
1206 aa	352	0.002	Consensus	No
	895	0.005	Consensus	No
	1077	0.014	Consensus	No
atToc120	52	0.008	Consensus	No
(At3g16620)	57	0.031	Consensus	No
1084 aa	209	0.05	Non-consensus	No
	777	0.006	Consensus	No
	959	0.013	Consensus	No
atToc90	191	0.027	Consensus	Yes
(At5g20300)	481	0.017	Consensus	No
793 aa	711	0.02	Consensus	No
	786	0.042	Non-consensus	Yes

atToc75 (At3g46740) 818 aa	434 513	0.049 0.029	Non-consensus Consensus	No No
atToc33 (At1g02280) 297 aa	291	0.044	Non-consensus	No
atToc34 (At5g05000) 313 aa	290 298	0.026 0.043	Consensus Non-consensus	No Yes

917

918

919 **Table 2**

920 **Primers used during the course of this study.**

921 (A) Primers used in restriction cloning procedures.

Primer name	Sequence*	Used to generate…
SCE1 F (HindIII)	AAAAGCTTATGGCTAGTGGAATCGCTC	pSAT4(A)-nEYFP-N1 SCE1
SCE1 R (EcoRI)	AAGAATTCGACAAGAGCAGGATACTGCTTG	pSAT4(A)-nEYFP-N1 SCE1
Toc159-5 F (EcoRI)	AAGAATTCAATGGACTCAAAGTCGGTT	pSAT4-cEYFP-C1-B Toc159
Toc159-3 R (SalI)	AAGTCGACTTAGTACATGCTGTACTT	pSAT4-cEYFP-C1-B Toc159
Toc132-5 F (XhoI)	AACTCGAGCTATG GGAGATGGGACTGAG	pSAT4-cEYFP-C1-B Toc132
Toc132-3 R (SmaI)	AACCCGGGTCATTGTCCATATTGCGT	pSAT4-cEYFP-C1-B Toc132
Toc33-5 F (HindIII)	AGAAGCTTCGATGGGGTCTCTCGTTCGT	pSAT4-cEYFP-C1-B Toc33
Toc33-3 R (XbaI)	AATCTAGATTAAAGTGGCTTTCCACT	pSAT4-cEYFP-C1-B Toc33
Toc34-5 F (HindIII)	AGAAGCTTCGATGGCAGCTTTGCAAACG	pSAT4-cEYFP-C1-B Toc34
Toc34-3 R (XbaI)	AATCTAGATCAAGACCTTCGACTTGC	pSAT4-cEYFP-C1-B Toc34
OEP7 F (XhoI)	CTCGAGATGGGAAAAACTTCGGGA	pSAT4(A)-cEYFP-N1 ΔOEP7
OEP7-35 R (KpnI)	GGTACCGGAATTTATCGAGGAAAGG	pSAT4(A)-cEYFP-N1 ΔOEP7

922

923

924 (B) Primers used in Gateway cloning procedures.

Primer name	Sequence*	Used to generate…
SCE1 Gateway F	GGGGACAAGTTTGTACAAAAAAGCAGGCTCCATGGCTAGTGGAATCGCTC	p2GWY7 SCE1
SCE1 Gateway R	GGGGACCACTTTGTACAAGAAAGCTGGGTTGACAAGAGCAGGATACTGC	p2GWY7 SCE1
SUMO1 Gateway F	GGGGACAAGTTTGTACAAAAAAGCAGGCTCCTCTGCAAACCAGGAGGAAGACAAG	p2YGW7 SUMO1
SUMO1 Gateway R	GGGGACCACTTTGTACAAGAAAGCTGGGTTTCAGGCCGTAGCACCACC	p2YGWY SUMO1
SUMO2 Gateway F	GGGGACAAGTTTGTACAAAAAAGCAGGCTCCTCTGCTACTCCGGAAGAAGAC	p2YGW7 SUMO2
SUMO2 Gateway R	GGGGACCACTTTGTACAAGAAAGCTGGGTTCTAAAAGCAGAAGAGCTTCAGGCC	p2YGW7 SUMO2
SUMO3 Gateway F	GGGGACAAGTTTGTACAAAAAAGCAGGCTCCTCTAACCCTCAAGATGACAAGCCC	p2YGW7 SUMO3
SUMO3 Gateway R	GGGGACCACTTTGTACAAGAAAGCTGGGTTTTAAAGCCCATTATGATCGAAAAGC	p2YGW7 SUMO3

925

926 (C) Primers used in RT-PCR experiments.

Primer name	Sequence*	Used to amplify…
SUMO1 F(2)	AAAAAGCAGGCTCCACAAAAGCCACGGCCAATTAG	*SUMO1*
SUMO1 R(2)	AGAAAGCTGGGTTCCATTCATATCACACACAAGCCC	*SUMO1*
SUMO3 F	ACAGACTGGAGTTTTTGTTTC	*SUMO3*
SUMO3 R	CTCATGAGTCATTTACACACACG	*SUMO3*
eIF4E1 F	AAGATTTGAGAGGTTTCAAGCGGTGTAAG	*eIF4E1*
eIF4E1 R	AAACAATGGCGGTAGAAGACACTC	*eIF4E1*
Siz1-HindIII-F	AAAAGCTTATGGATTTGGAAGCTAATTGTAAG	*SIZ1* (for *siz1-4*)
Siz1-seq-1R	TCTGCATTGTGCTTGCAC	*SIZ1* (for *siz1-4*)
Siz1-F	GGATTATCTTCCAGTAATAGGCAAG	*SIZ1* (for *siz1-5*)

Siz1-R	CCCGACTGAGCTGAAGCATC	*SIZ1* (for *siz1-5*)

927

928 (D) Primers used to genotype mutants.

Primer name	Sequence	Used to genotype…
SUMO1 F(2)	AAAAAGCAGGCTCCACAAAAGCCACGGCCAATTAG	*sum1-1*
SUMO1 R(2)	AGAAAGCTGGGTTCCATTCATATCACACACAAGCCC	*sum1-1*
SUMO2 F	CGTTGTTGGTACTTGGTTGG	*sum2-1*
SUMO2 R	CAAAACTCTAAACTGGTCGG	*sum2-1*
SUMO3 F	ACAGACTGGAGTTTTTGTTTC	*sum3-1*
SUMO3 R	CTCATGAGTCATTTACACACACG	*sum3-1*
SCE1 F	CGCCGCGAAATCTGGACC	*sce1-4*
SCE1 R	TTCCTCTCTTCAGCTAAACG	*sce1-4*
SIZ1 F(2)	GCAAACAGGGAAAGAAGCAGG	*siz1-4*
SIZ1 R(2)	CATTGAGTCTGTTTCTAGCG	*siz1-4*
LBb1	GCGTGGACCGCTTGCTGCAACT	SALK lines (left border)
LB1	GCCTTTTCAGAAATGGATAAATAGCCTTGCTTCC	SAIL lines (left border)

929

930 (E) Primers used to map the *siz1-4* and *siz1-5* T-DNA insertions.

Primer name	Sequence	Used to map…
Siz1-Seq-1R	TCTGCATTGTGCTTGCAC	*siz1-4* T-DNA insertion
Siz1-Seq-3R	TGACAACCACTGTATGCAGG	*siz1-5* T-DNA insertion

931

932 * Underlining indicates restriction sites (A and C), or attB1 and attB2 recombination sequences (B).

933

Additional files

Source data 1

Immunoblot source data.

Uncropped immunoblot images for Figures 1 and 5, and their supplements.

Transparent reporting form